Modeling of Opening Characteristics of an Atrium in Natural Ventilation

by

Qinzi Luo

Submitted to the Department of Architecture
in partial fulfillment of the requirements for the degree of

Master of Science in Building Technology

at the

MASSACHUSETTS INSTITUTE OF TECHNOLOGY

February 2018

Author .....
Department of Architecture
January 15, 2018

Certified by .....
Leon R. Glicksman
Professor of Building Technology and Mechanical Engineering
Thesis Supervisor

Accepted by .....
Sheila Kennedy
Professor of Architecture
Chair, Departmental Committee for Graduate Studies

Modeling of Opening Characteristics of an Atrium in Natural Ventilation

by

Qinzi Luo

Submitted to the Department of Architecture
on January 15, 2018, in partial fulfillment of the
requirements for the degree of
Master of Science in Building Technology

Abstract

Atriums are widely applied in non-residential buildings to provide social contact, daylight, air circulation, and aesthetic requirements. Buoyancy-driven ventilation systems are common because they can maintain suitable thermal comfort and reduce energy. Modeling techniques used to simulate naturally ventilation include analytical models, full-scale and small-scale experiments, computational fluid dynamics(CFD) and airflow network tools, which have advantages and limitations. Investigations on atrium structure and opening characteristics have been limited up to now.

This thesis studies the temperature stratification and air flow rates inside atrium buildings in purely buoyancy-driven ventilation. Ventilation effects in models with different heat sources, opening locations, opening sizes and numbers of floors are compared using CFD simulations. An airflow network tool, CoolVent, is used to compare the results with CFD models. Both temperatures and flow rates match well with discrepancies less than 10%. Therefore, the well-mixed temperature assumption in the atrium in the airflow network tool is suitable for single-layer atrium buildings. The full-scale experiment provides a detailed data set for further investigations. Air temperatures keep stable on every floor but increase with height. Therefore, the well-mixed temperature assumption over the entire height of the atrium in many analytical models is not applicable when the cross section of the atrium is small. The prediction of temperature distribution and flow rates in atrium buildings with buoyancy-driven ventilation is provided in details. Indoor air temperatures and flow rates can be calculated with known outside air temperatures and surface temperatures in the atrium. The estimation of heat transfer coefficients, especially the approximation of stairs can cause some discrepancies between calculated and actual results.

Thesis Supervisor: Leon R. Glicksman
Title: Professor of Building Technology and Mechanical Engineering

Acknowledgments

I am tremendously grateful for the many advisors, colleagues, collaborators, friends and parents who made this thesis possible. First, I want to express my gratitude to my academic and research advisor, Professor Leon R. Glicksman. His sharpness, enthusiasm, energy and breadth of skills and knowledge in the fields of natural ventilation and energy-efficient building components and design, influence and guide me throughout the research process. It is impossible to list here all he has taught me and helped me in study and life. I will never forget the experience of working with and learning from him.

I want to thank all faculties, staffs and students in the Building Technology Laboratory. I am grateful for the encouragement, thoughtful feedback, and technical assistance of Professor Les Norford, Christoph Reinhart, Caitlin Mueller, and John Ochsendorf. I want to thank our Departmental Administractor Kathleen Ross for the help and assistance for me. I also want to thank Alonso Dominguez Espinosa, who gave me helpful advice on research and technical problems about computational fluid dynamics. I am thankful for my friends, Jiamin Sun and Yijiang Huang, who helped me to complete the full-scale experiments and gave me unconditional support throught the two years in my life and study. More broadly, I am thankful for all other Building Technology students with research areas outside of my own, especially Alpha Yacob Arsano, Shreshth Nagpal, Tianyi Chen, Johnathan Kongoletos, Jiachen Mao, Paul Mayencourt, and Nathaniel Jones. They helped me understand other aspects of building design and technologies and gave me a friendly, engaging and intellectually environment in the laboratory.

I have relied on the consistent and unconditional support of my family to finish the challenging study and research at MIT. I deeply appreciate and love them.

Contents

List of Figures

List of Tables

Chapter 1

Introduction

1.1 Development of Atriums

Atriums, large open air spaces or skylights in covered space surrounded by buildings as shown in Fig.1-1, have been widely used, especially in non-residential buildings. Atriums provide aesthetic appeal, exposure for daylight, socialization and air flow among the stories of the buildings. This architectural feature has often been adopted for aesthetics in different regions and climates without consideration of suitable conditions, materials, environmental potentials (radiation, wind and others) and energy consumption especially in ancient times. The earliest traditional atrium can be traced back to 3000 BC in a remain of a house in Ur, Mesopotamia as a central courtyard[8]. During the Industrial Revolution, atriums with plate glass and slender structural elements of iron and steel were applied in the design of buildings. Until late 1950s and early 1960s, modern atriums became popular[9].

Figure 1-1: Photographs of atriums[1].

The generic forms of atriums always depend on functions of the buildings, thermal and ventilation expectations, daylighting performance, climate conditions, and architectural considerations. The displacement of the atriums in building is important to determine the potential environmental benefits. Four shapes of atriums are widely accepted as shown in Fig.1-2[10]. Each form is chosen according to the local climates, daylight requirements, ventilation and other demands. Atriums are set at one side of buildings as a glazed facade to get attractive views and solar gains in winters for temperate climates. In hot and humid climates, centralized and linear atriums are always used to minimize temperature fluctuations during hot seasons. Furthermore, Temperature fields of all atrium types are the closest in neutral climate. Centralized and linear atriums are still the most popular generic types now[2].

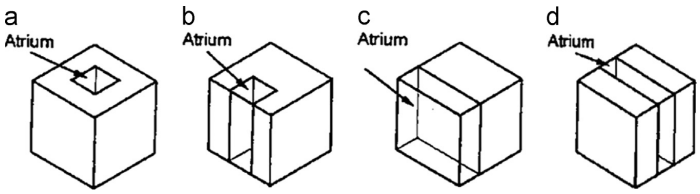

Figure 1-2: Four forms of atriums. (a)centralized, (b)semi-enclosed, (c)attached, (d)linear[2].

(a) The centralized Atrium[11] (b) The semi-enclosed atrium[12]

(c) The attached atrium[13] (d) The linear atrium[14]

Figure 1-3: Photographs of four different typical atriums.

1.2 Application of Natural Ventilation

Natural ventilation has become a key method to provide optimum indoor air circulation, create suitable thermal environments and maintain appropriate mechanical systems, such as HVAC. Fig.1-4 shows a schematic of typical buoyancy-driven ventilation in an atrium building. One main reason for using natural ventilation is its potential to reduce building energy use. The operation of buildings consumes about 40%(or about 39 quadrillion British thermal units) of national energy in the USA[15], 23% of which is for cooling and ventilation[4]. Thus, pure natural ventilation, which creates air flow without mechanical systems, substantially saves energy use in cooling and ventilation.

Another key reason when applying the natural ventilation is indoor thermal comfort. Clothing, lighting, radiation from walls, activity level, air speed, and many other factors have been recognized to decide the thermal comfort environment. The American Society of Heating, Refrigerating and Air Conditioning Engineering(ASHRAE) provides some adaptive ranges of operative temperatures or humidity ratios based on the clothing amount or mean outdoor air temperatures. Researchers also conducted many comparative experiments on indoor comfort for people living in air conditioning buildings and purelly naturally ventilated buildings[16].

Based on 22,000 sets of data collected from 160 buildings, Brager found that people living in naturally ventilated buildings likely felt comfortable in a wider range of air temperatures, when they were at near sedentary activity levels, could freely control openings and adapt their clothing anytime during the year. But defining suitable thermal comfort conditions quantitatively is still contentious.

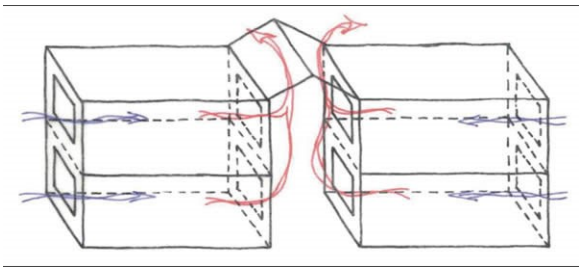

Figure 1-4: Schematic of typical buoyancy-driven ventilation in an atrium building[3].

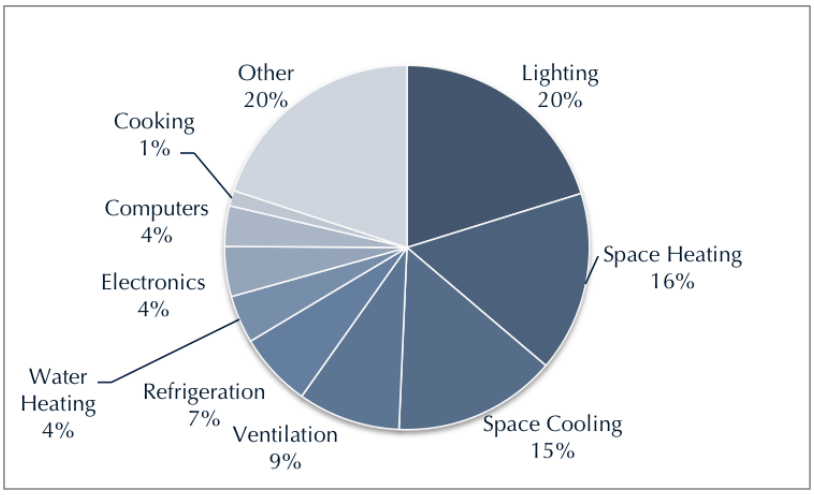

Figure 1-5: 2011 U.S.buildings energy end-use split[4].

1.3 Natural ventilation modeling strategies

The current modeling methods are outlined below. These techniques are classified into four groups, each of which is discussed in this chapter: analytical models, full-scale and small-scale experiments, CFD(computational fluid dynamics) models and airflow network models.

1.3.1 Analytical models

Buoyancy-driven ventilation is created by a hydrostatic pressure gradient created by density differences. Fig.1-6 shows a simple buoyancy-driven ventilation model which is a single zone with two equal area windows at elevations z_1 and z_2, a uniform indoor temperature T_{in} and ambient temperature T_{out}, and negligible wind. The indoor air is warmer than the outdoor air due to internal heat gains[17].

The column height and gravitational acceleration are equal inside and outside. Thus, the hydrostatic pressure varies only with density. Because warmer air is less dense than cool air, a smaller pressure gradient exists inside than outside, which is shown in Fig.1-7.

The lower opening has a higher pressure outside than inside, which draws air into the building, while the upper opening has a higher pressure inside than outside, which

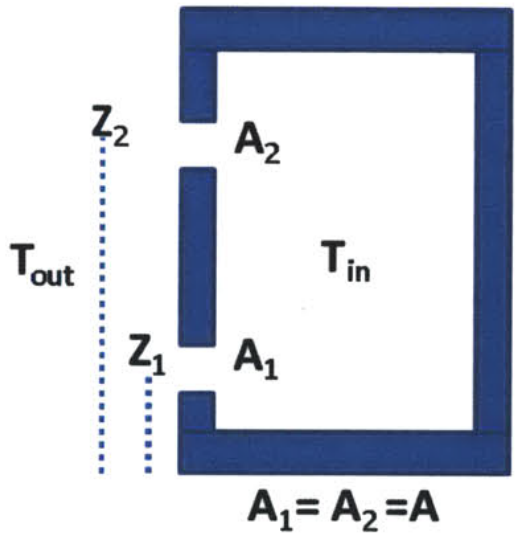

Figure 1-6: Example of simple buoyancy-driven ventilation.

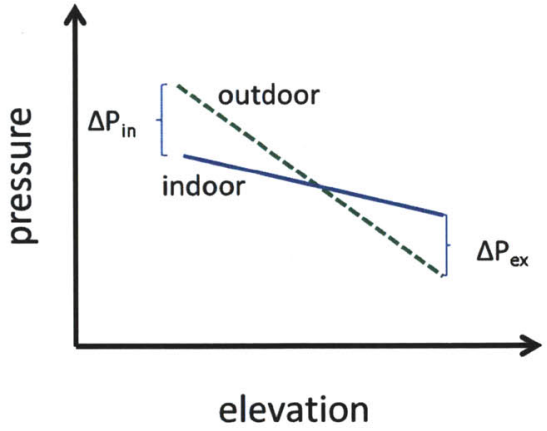

Figure 1-7: Indoor and outdoor pressure gradients as a function of elevation in purely buoyancy-driven ventilation.

drives air out of the building. Using ideal gas law and Bernoulli equation, the driving pressure can be obtained:

$$(P1 - P2)_{out} - (P_1 - P_2)_{in} = \rho_0 g(z_2 - z_1)\frac{T_{in} - T_o}{T_{in}} \tag{1.1}$$

where g is the acceleration in m/s^2, P_{in} is the indoor pressure in Pa, and P_{out} is the outdoor pressure in Pa. The volume flow rate of unidirectional flow through an opening of area A depends on the driving pressure drop ΔP across it with the orifice

equation:

$$V_{orifice} = AC_D\sqrt{\frac{2\Delta P}{\rho}} \tag{1.2}$$

where C_D is the discharge coefficient. Assuming both openings have the same area A and discharge coefficient C_D, and combining the orifice equation and Bernoulli equation, the flow rate entering the building can be obtained:

$$V_{buoyancy} = AC_D\sqrt{\frac{g(z_1 - z_2)(T_{in} - T_o)}{T_{in}}} \tag{1.3}$$

Fitzgerald and Woods [18]developed a more complicated model of a room where there is a distributed heat load Q_H at the base of the room leading to vigorous convection and a well-mixed interior . The basic theorem of conservation of momentum and energy were used to calculate the temperature elevation ΔT and flow rate V. They also assumed two openings A and B on the side walls at different height h_A and h_B. The buoyancy driving the flow is related to the column of room air extending from the height of B to the height of A. The reduced gravity is g^*, defined as $g^* = g(\rho_e - \rho_r)/\rho_e$, where the ρ_e and ρ_r are the density of the exterior and interior air, and g is gravitational acceleration. Assuming the effective area of the two vents is A^*, defined as $A^* = c_A a_A c_B a_B/(0.5(a_A^2 a_A^2 + c_B^2 a_B^2))^{0.5}$ where a_A, a_B are the areas of vents, and c_A and c_B are the loss coefficients. The flow rate V is given by

$$V = A^*\sqrt{g^*(h_A - h_B)} \tag{1.4}$$

where the effective opening area is A^*.

The heat flux Q_H is given by balance of energy input:

$$Q_H = \rho C_p \Delta T V \tag{1.5}$$

where ΔT is the temperature elevation in the room, ρ is the density of air and C_p is the specific heat capacity. The reduced gravity can be written as:

$$g^* \sim g\beta\Delta T \tag{1.6}$$

where the coefficient of expansion for air is $\beta = 1/T$. The temperature elevation in room is:

$$\Delta T = \left(\frac{{Q_H}^2}{\beta\rho^2{C_p}^2 A^{*2} g(h_A - h_B)}\right)^{1/3} \tag{1.7}$$

The volume flow rate in room is:

$$\Delta V = \left(\frac{A^*(h_A - h_B)g\beta Q_H}{\rho C_p}\right)^{1/3} \tag{1.8}$$

Although the analytical models require few computing resources and are rich in physical meanings, they are difficult to use in real cases because the simple geometries cannot describe the actual buildings even with many reasonable assumptions, especially the assumption of a uniform temperature in the space.

1.3.2 Full-scale and small-scale experiments

Actual-size replications of the prototype buildings are always used to provide rich insight into the air flow. To provide well distributed air flow throughout the building, the proportion of areas of inlets and outlets is important.

Full scale models can provide accurate modeling methods without exact physical expressions. However, this method is extremely resource-intensive and results can only be applied to similar building structures. Although there are already some full scale experiments, complete and systematic data sets are still lacking. Meanwhile, most visualization techniques for indoor air flow include some buoyancy created by the visual materials such as smoke that are inconsequential in inertial-dominated flow.

Some reduced-scale experimental results[19] show that the ambient temperatures obviously affect the temperature distribution of the atrium space. They used four different ambient temperatures (20 ℃, 25 ℃, 30 ℃and 35 ℃), which represent the mean noon temperature of winter, spring, autumn and summer respectively. Results show that different outdoor temperatures have different influences on indoor temperature distributions. The buoyancy-only natural ventilation can be utilized for an atrium space to reach the general thermal comfort level in a hot and humid climate only

in spring and winter, or when the outdoor temperature being under 30℃. However, the efficiency of stacks is limited when ambient air temperature is higher than 35℃. Therefore, the efficiency of buoyancy-driven ventilation in a hot and humid climate has to be applied to a high building to induce a sufficient pressure gradient.

Reseachers also developed some different methods to construct reduced-scale model. The filling box experiment[5], which is also called the small-scale salt bath experiment, uses liquids of different densities to replace the cold and warm air in a small container. Fig.1-8 shows the box filled with dense fluid and lowered into a large reservoir of fresh water.

This experiment clearly simulates the buoyancy effects on a small scale and achieves good visualization. Yet, due to the opaque properties of water and transparent features of air for infrared radiation, the filling box method ignores radiation between the floor and ceiling, the most important part of heat transfer in this case, leading to inaccurate results.

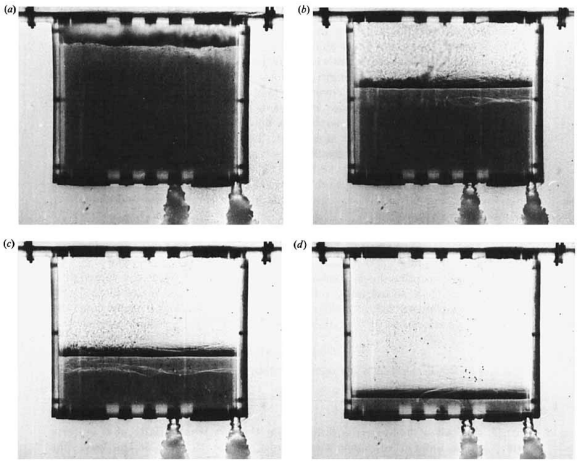

Figure 1-8: Displacement flow from a box initially containing dense fluid. The box was filled with dense fluid and lowered into the large reservoir of fresh water. Four large plugs (diameter 5.5 cm) were removed from the top of the box, and the experiment was started by removing two small plugs (diameter 1.8 cm) from the bottom of the box. The photographs are at (a) t/t_E , = 0.07, (b) 0.29, (c)0.50 and (d) 0.86. The emptying time t_E, is 139 s. Note the descending sharp interface between the clear, ambient fluid and the dark, dense fluid. These and subsequent photographs are of side views using the shadowgraph technique: the dense fluid is dyed[5].

Dimensionless analysis is necessary in small scale experiments. All variables ap-

pear as ratios where dimensions are canceled, creating dimensionless parameters. For buoyancy dominated flow, the Grashof number, Gr, and Prandtl number, Pr should be equal. When buoyancy-driven and wind-driven effects are both important, the Archimedes number, Ar, Gr and Pr should be the same.

Therefore, small scale models can simulate full-scale behaviors using significantly fewer sources to construct and measure air flow. However, as Nielsen[20] recognized, if the scale of a building is reduced by a factor of 10, the velocity should be increased by a factor of 10 to remain the same Reynolds number, which would lead to an increase in the temperatures difference by 10 to get the Archimedes number.

It is impossible for all dimensionless parameters to be the same because of their interdependence, even though some threshold values are raised for special conditions where those parameters are not equal. Good solutions and justification are still needed.

1.3.3 Computational fluid dynamics models

Computational fluid dynamics(CFD) models solve many partial differential equations for the conservation of mass, momentum and energy using computational sources. Y.Ji[21] did the steady-state simulations of natural ventilation in a single-storey space connected to an atrium. The results showed good agreement between the mathematical models, experiments and CFD predicting non-dimensional volume rate and buoyancy force, but had obvious discrepancies in neutral plane height. They also clarified that an atrium may fail to enhance the air flow when the resistance of openings overcomes the enhancement.

M.Alejanda et al.[6] applied the CFD models shown in Fig.1-9 and Fig.1-10 to conclude that neglecting radiation results in considerably higher excess temperatures for heated surfaces, lower temperature of non-heated surfaces and the occupant zone. In pure buoyancy-driven ventilation, the reduction of air temperatures can lead to underprediction of the overall flow rate of 6% but much larger errors in the temperature distribution. Therefore, desired thermal and flow performance cannot be achieved to predict thermal comfort.

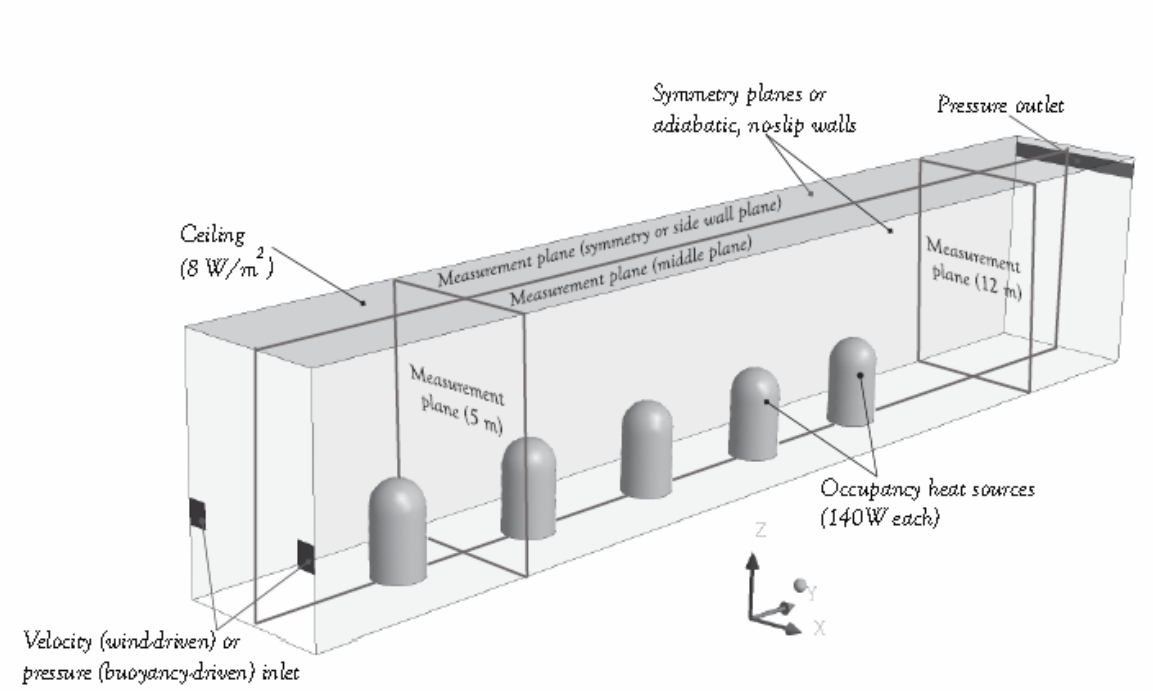

Figure 1-9: Configuration of a large room. All heated surfaces (occupancy and ceiling) were treated as constant heat flux surfaces[6].

In addition, vapor and carbon dioxide in the air have several infrared bands absorbing and emitting radiative energy. They are important for large spaces. Yet, radiation effects in buildings with high humidities are rarely considered in current CFD studies [22].

C.A.Rundle et al.[23] provide some validation of a commercial CFD code against experimental measurements. Results show that the k-w turbulence model can simulate fluid flow and heat transfer in turbulent natural convection flow and a discrete transfer radiation model can model radiation with a coarse mesh.

In short, CFD models have been validated and can model arbitrary geometries, but they can focus only on a short time period. For annual ventilation prediction, CFD is not suitable. Furthermore, its application requires knowledge of fluid mechanics, fundamental computational power and detailed consideration of inertial conditions.

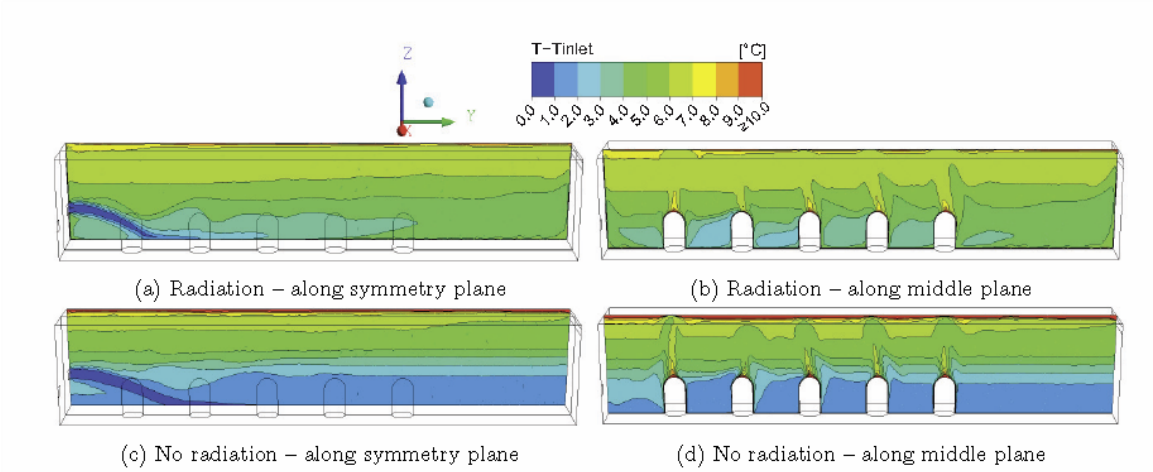

Figure 1-10: Large open room under buoyancy driven flow. Excess temperature when (a) and (b) accounting for radiation, and (c) and (d) neglecting radiation. Results are shown along (a) and (c) the plane of symmetry, and (b) and (d) the middle plane[6].

1.3.4 Airflow network models

Airflow network models are popular to predict airflow rates and temperatures in naturally ventilated buildings[24]. The models divide a building into many zones or nodes and generate a network among them based on the architectural design. A power-law function is applied to calculate the flow rates F_{ij} between connected zones i and j:

$$F_{ij} = C_{ij} A_{ij} |\frac{\Delta P}{\rho}|^{n_{ij}} \tag{1.9}$$

where ΔP is the pressure drop across the zones, n is the flow exponent, A_{ij} is the cross section area connecting two nodes, and C_{ij} is the flow coefficient. Mass conservation gives that

$$\sum_j F_{ij} = 0 \tag{1.10}$$

Energy conservation for each nodes is

$$\sum_j Q_{ji} + Q_{source} + Q_{boundary} = \rho_i V_i C_p \frac{\partial T_i}{\partial t} \tag{1.11}$$

where Q_{ji} is the energy flux from node j to current node i, Q_{source} is the heat generated

at node i, $Q_{boundary}$ is the heat transfer of boundaries, v_i is the volume of air, C_p is the heat capacity, and T_i is the temperature at node i. Luo et al.[25] and Rousseau et al.[26] coupled airflow and thermal models in their airflow network models to predict flow rates and temperatures. MIT developed an application called CoolVent by using airflow network models which has been validated by CFD models[27].

Airflow network models can predict the flow rates and temperatures of natural ventilation in any arbitrary buildings because they convert the complex structure into simple networks of nodes. However, they are limited by many key assumptions. They ignore the momentum of air assuming small air velocities. And they assume a well-mixed condition with an uniform temperature in each zone. Obviously, models are questionable when air exchange rates are really high or uneven heat sources exist in the space.

1.4 Summary of current natural ventilation modeling methods

In conclusion, analytical models are rich in physical meaning but too simple to use in real world situations. The experimental results reflect real conditions without many assumptions. Yet, they are too source intensive to be used widely. More data sets are still need because of a small number of conducted experiments.CFD models accurately simulate natural ventilation but require long run times.

The investigations focusing on the operating characteristic of atriums have been limited up to now. The full scale experiment provides a more detailed data set than any published work. Robust CFD simulations are also used to investigate the opening characteristics with different settings. The research on enhancing experimental models and CFD methods reported here will help designers and engineers to decide the opening design in naturally ventilated buildings.

1.5 Thesis objective

The aim of this research is to study the temperature stratification and the air circulation inside the atrium space in purely buoyancy-driven ventilation through field experiments, analytical calculations and computational fluid dynamics simulation, and analyze the physical insight of the ventilation process by taking influencing factors in to consideration. Specific contributions are summarized below.

Because the assumption of a uniform temperature inside the atrium in most analytical work cannot reflect the actual situation, a full scale experiment in a stairwell was conducted with more details than most published work to understand the real situations of buoyancy-driven ventilation in an atrium space. Better data sets can be extracted especially the temperature stratification at different heights, temperature and flow rate changes with different opening areas.

Calculations and analysis are investigated to explain the temperature and flow rate changes during ventilation process. The influence of many factors can be determined from the comparison of calculations and measured data.

Computational fluid dynamics(CFD) models are used to visualize and understand how airflow establishes in many scenarios: different heat sources, sizes and locations of openings.

Operating characteristics of typical atrium buildings will be illuminated and integrated into the natural ventilation design tool"CoolVent" .

This thesis would help engineers and architects to make informed decisions on the expected thermal environment and air flow conditions .

Chapter 2

CFD models of atrium buildings in buoyancy-driven Ventilation

Design and prediction of natural ventilation is difficult due to the unsteadiness of the buoyancy effects, complex architectural structures and the coupling between the temperature and flow rate changes. Simple analytical models and field experiments are not enough to study the ventilation effects in buildings with different opening and structure features. But CFD models could easily simulate those complex cases and give detailed comparable results. This chapter investigates computational fluid dynamics(CFD) models to study the purely buoyancy-driven ventilation inside an atrium building with different heating sources, opening locations and sizes, and the number of floors.

2.1 Basic building model

As discussed in the introduction chapter, centralized atriums, which has an outlet at the middle of the top and connect to other rooms around, are still the most popular generic types now. The building model used in CFD simulations in this chapter, as shown in Fig.2-1 has one floor(8 m length by 6 m wide by 4 m high), which is assumed to be a large single room. The room is connected to a 10 m-high single ventilation atrium, whose floor area is 24 m^2(6 m$\times$4 m). A 2 m^2 inlet on the south wall of

the room allows outdoor air to enter the room. A 2 m^2 opening from the room to the atrium allows air to exit the room. Then the air goes through the 2 m by 2 m exhaust opening on the top of the atrium at the middle. One vertical measuring plane is located at the symmetry plane of the whole zone, orthogonal to the openings on the room wall, as shown in the Fig.2-1.

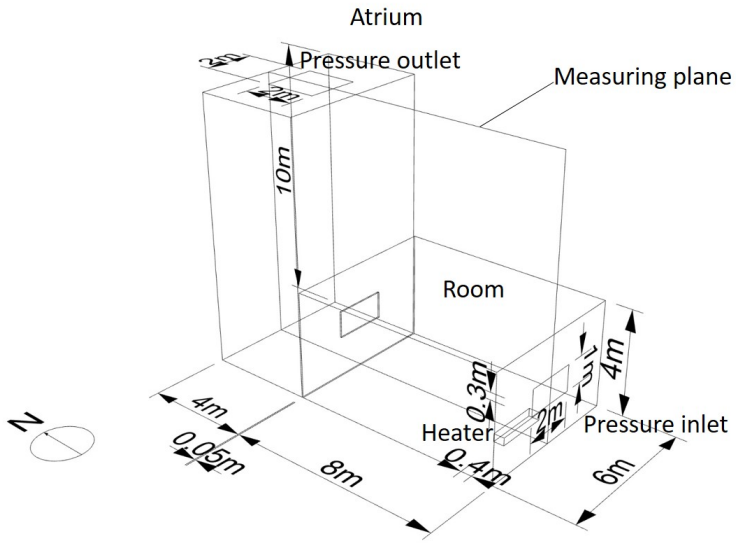

Figure 2-1: Geometry of the one storey atrium building with an heater near the wall simulated with CFD for case A, B and C. One vertical measuring plane is located at the symmetry plane of the whole zone.

2.2 Description of CFD settings

Many cases are simulated in a transient mode by ANSYS Fluent, the most powerful computational fluid dynamics software tool available. The cases are assumed to reach a steady state when the bulk exhaust temperature varies less than 0.003 °C for 1000 iterations. The kϵ RNG turbulent model is used based on its good performance of accurately simulating air dynamics in actual building scales[17]. The radiation is accounted for using a surface to surface (S2S) model with a residual convergence criteria of 0.001, which assumes the indoor air is transparent. All surfaces inside are simplified with an emissivity of 1.0. This simplification is justified given typical mate-

rials in a room, excluding polished metals, with a emissivity above 0.9[28]. The mesh density increases near openings and near walls with $y^+ \leq 5$ in accordance with the enhanced wall functions. The enhanced wall functions with enhanced thermal effects and buoyancy effects are also considered. To study the pure buoyancy-driven ventilation, the ambient is windless with air temperature of 293.15 K. Therefore, initial reference and operation temperatures for all zones are 293.15K.

Adiabatic boundary conditions are set to all surfaces except the floors on each floor. The outlet on the top of the atrium is modeled with a "pressure outlet" condition while the inlet of the room is modeled with a "pressure inlet" condition under the same specific temperature of 293.15K, although the reverse flow at the outlet is never predicted.

The "PRESTO!" (PREssure STaggering Option) scheme is used for pressure interpolation, while the "SIMPLE" (Semi-Implicit Method for Pressure-Linked Equations) algorithm is used for velocity-pressure coupling. Spacial discretization of governing equations is achieved using a second-order upwind scheme.

In buoyancy-driven ventilation, the heat sources inside are always important to enhance the air flows. In current buildings, the heat sources in a room are always simulated as a heater near the corner or distributed heat sources on the floor. Different heat source types would lead to different air flow and temperature fields. In this study, a CFD investigation is applied to explore and compare the influence of the heat sources in a typical full-scale building.

The effects of heat sources are explored by changing the boundary conditions. Two sets of boundary conditions are considered: 1) two different heaters with constant and uniform heat fluxes over the heater surface; 2) a floor with evenly distributed heat loads. In the first setting, the power of the larger heater is 1.68 kW(a typical setting, case A) while that of the smaller heater is 1.12kW(case B). In the second setting, the heat load of the floor is 30 W/m^2(case C), according to the heat loads in standard office buildings in USA[29], which achieves the same heat intensity as the smaller heater condition,1.12kW.

Table 2.1: Boundary conditions of CFD cases with different heat sources

Initial temperatures(K)	Room	Atrium	Large Heater(case A)	Small Heater(case B)	Floor heating(case C)
Ambient/ Room/Atrium	Walls/Floor /Ceiling	Walls/Floor /Ceiling	Heat flux	Heat flux	Heat flux
293.16/300/300	Adiabatic	Adiabatic	1.68kW	1.12kW	$30W/m^2$

The geometry in the study of the atrium opening characteristics and CFD settings are similar to the models discussed above. Considering general heat sources in real buildings and simplifying the mesh, we apply the uniformly distributed heating flux to all following simulations. All other boundary conditions are the same as models above. To study the features of the outlet on the top of atrium, the CFD model contains a building model and a large ambient zone outside to compare the air flows from the outlet, which is shown in Fig.2-2. In the ambient zone, three surrounding sidewalls are set as pressure inlets and the ceiling is set as a pressure outlet. And the floor is modeled as an adiabatic no-slip boundary. Temperatures of all surfaces in the ambient zone are 293.15 K.

The connecting opening types and the exhaust opening locations of the atrium are varied through the simulations in this comparison group. Two types of connecting openings are modeled: a window at the middle(2 m wide and 1 m high) and a floor-to-ceiling opening(6 m wide and 4 m high). In addition, the outlets on the top of the atrium with three different locations which are shown in Fig.2-3 are modeled: a middle opening, a south opening adjacent to the south atrium wall, and a north opening adjacent to the north atrium wall.

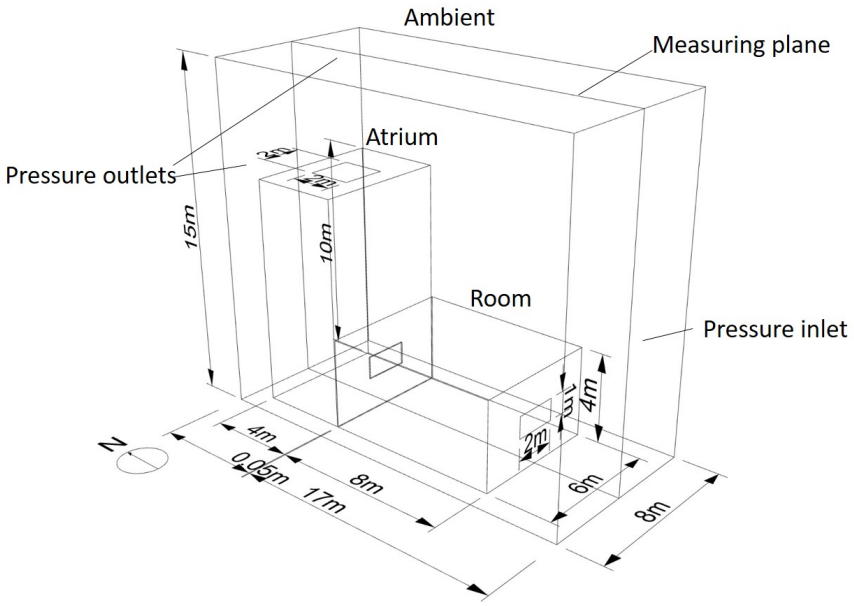

Figure 2-2: Geometry of the one storey atrium building with uniformly distributed heat loads simulated with CFD for case D-L. One vertical measuring plane is located at the symmetry plane of the whole zone.

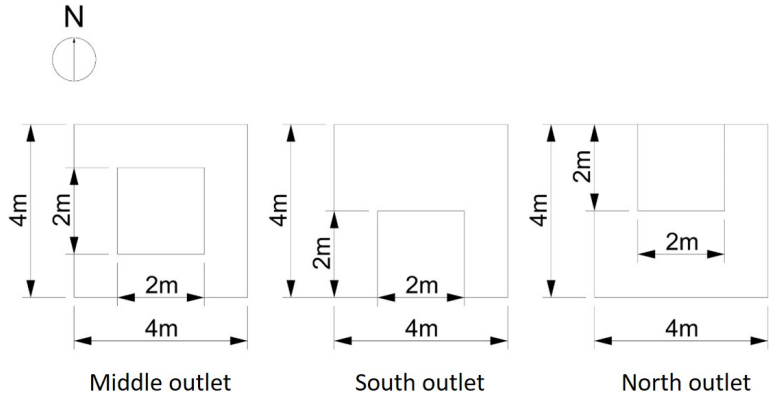

Figure 2-3: Schematics of the top of the atriums with the middle outlet, south outlet and north outlet.

The outlet size is another important factor that would apparently affect ventilation effects. A 2 m by 1 m connecting window between the room and the atrium and a middle outlet at the top of the atrium are assumed for the first three cases with different cross section areas in this comparison group. Figure 2-4 shows the schematics of the top of the atriums with the original outlet, small outlet and large outlet.

Table 2.2: Boundary conditions of simulation cases with different connecting openings and outlet locations

case	Connecting opening	Outlet of the atrium	Initial condition	Ambient	Room /Atrium
			Tambient/Troom /Tatrium	Pressure inlet/outlet	Walls/Floor /Ceiling
D	A window	A middle opening	293.16K/300K /300K	Windless, 293.16K, zero gauge pressure	Adiabatic
E	A window	A south opening	293.16K/300K /300K	Windless, 293.16K, zero gauge pressure	Adiabatic
F	A window	A north opening	293.16K/300K /300K	Windless, 293.16K, zero gauge pressure	Adiabatic
G	A floor-to-ceiling opening	A middle opening	293.16K/300K /300K	Windless, 293.16K, zero gauge pressure	Adiabatic
H	A floor-to-ceiling opening	A south opening	293.16K/300K /300K	Windless, 293.16K, zero gauge pressure	Adiabatic
I	A floor-to-ceiling opening	A north opening	293.16K/300K /300K	Windless, 293.16K, zero gauge pressure	Adiabatic

Table 2.3: Boundary conditions of simulation cases with different outlet sizes

case	Connecting opening	Outlet of the atrium	Initial condition	Ambient	Room /Atrium
		Size	Tambient/Troom /Tatrium	Pressure inlet/outlet	Walls/Floor /Ceiling
J	A window	2m×2m	293.16K/300K /300K	Windless, 293.16K, zero gauge pressure	Adiabatic
K	A window	3m×3m	293.16K/300K /300K	Windless, 293.16K, zero gauge pressure	Adiabatic
L	A window	1m×1m	293.16K/300K /300K	Windless, 293.16K, zero gauge pressure	Adiabatic

Flooring heating of 60 W/m^2 at the ground of the room assists the buoyancy effect, and all other surfaces are set adiabatic. All other settings are the same as the models above(Case D, E, F). Boundary conditions of different cases are given in Table 2.3.

Because there are usually more than one floor for actual atrium buildings. Another two-storey building model which is shown in Fig.2-5 is also simulated to investigate differences between floors and the enhancement of the overall ventilation. The second room is added on the top of the original room with the same flooring heat loads. All other settings are the same as case J.

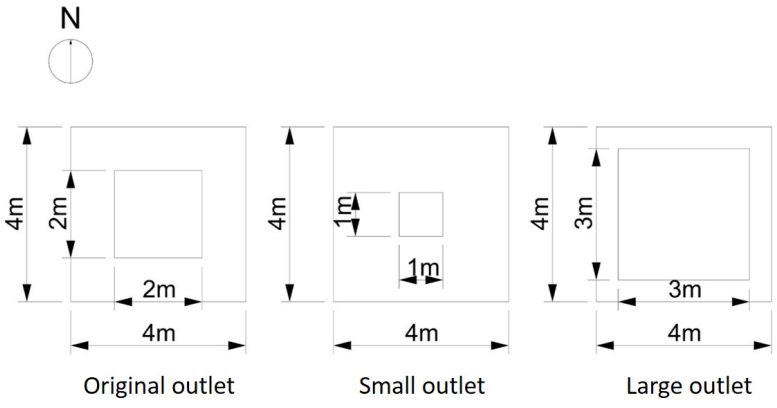

Figure 2-4: Schematics of the top of the atriums with the original outlet, small outlet and large outlet.

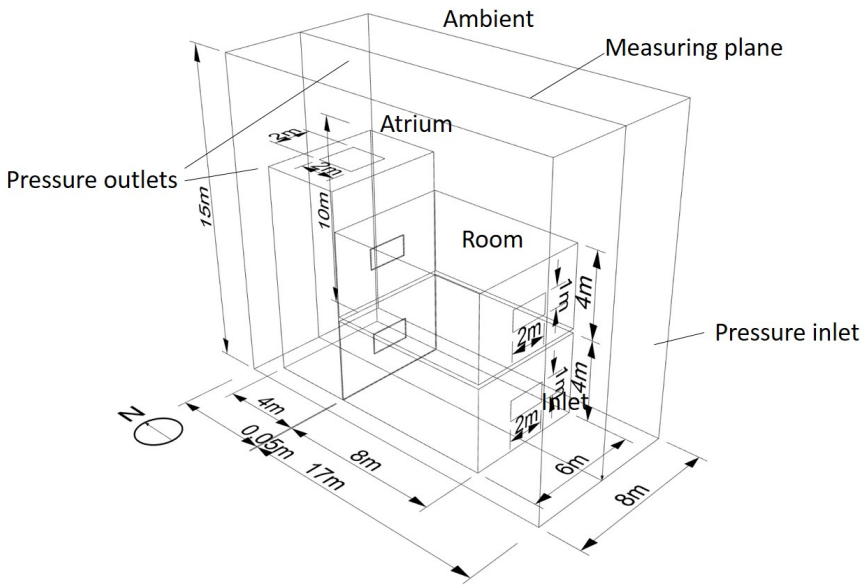

Figure 2-5: Geometry of the two storey atrium building with uniformly distributed heat loads simulated with CFD. One vertical measuring plane is located at the symmetry plane of the whole zone.

2.3 Results

All cases are simulated using computational fluid dynamics transiently until a real time more than 1000 seconds with a initial time step of 0.5s and automatically adjusted time intervals when the change of values remain less than 0.1%, which is close to the steady state. Figure 2-6 gives the plots of the streamlines in case A at different times (t = 10, 25, 100, 250 and 500 s) at the vertical measuring plane. Different colors refer to different particles. All particles are released at the inlet of room. Initially, when the heater has not heated up the inner space, the particles runs in clear and approximately parallel tracks passing through openings. Gradually, because of the strong buoyancy effect caused by the heater and collisions with boundaries, the trajectories are disturbed, mixed and in chaos.

Figure 2-7 show the velocity fields at different time(t = 10, 25, 100, 250 and 500 s). Obviously, the velocity directions change with time. Air comes from the inlet and falls down due to the gravity, while air near the heater is heated and floats up due

to the buoyancy effect. After passing the connecting opening between the room and atrium, most fluids hit the atrium wall and form a updraft going out of the atrium. Initially, the velocities at openings are high (up to 1.5 m/s) due to the sudden heat loads inside and temperature differences. Gradually, air velocities decrease and reach to a relatively steady state.

Fig.2-8 shows the temperature field change in this period, which also reflects the air flow change. Before 10 s, the temperatures in the atrium are uniform and steady. After 100 s, the heater near the wall generates a wall-attached plume along the sidewall and then the ceiling. Therefore, the temperature of the ceiling is very high. The upper hot flow and lower cool flow approximately divide the space to two layers finally. Temperatures are similar in most space of the atrium without a clear plume.

As mentioned above, three different heat sources are considered: a large heater with constant heat fluxes(1.68 kW), a small heater with constant heat fluxes(1.12 kW), a floor with evenly distributed heat loads($30W/m^2$). As shown in Fig.2-9, the velocity fields at the middle measuring planes of three cases at steady states are very similar. The larger heater leads to higher flow rates than those of the smaller heater. The heated floor (case C) performs higher flow velocities at the connecting opening, more mixed temperature fields in the inner space and an obvious plume in the middle of the atrium.

Fig.2-10 shows the temperature fields of three cases at steady states. Buoyancy-driven natural ventilation is established for all cases with different heat sources. The thermal plumes are generated through the convective heat exchange uniformly between air and the floor in the heated floor case. In the heater cases, high-momentum high-temperature plumes from heater surfaces are generated to drive the ventilation. The heater leads to a two-layer temperature stratification in the room and a plume with higher temperature from the connecting opening hitting the atrium sidewalls directly.

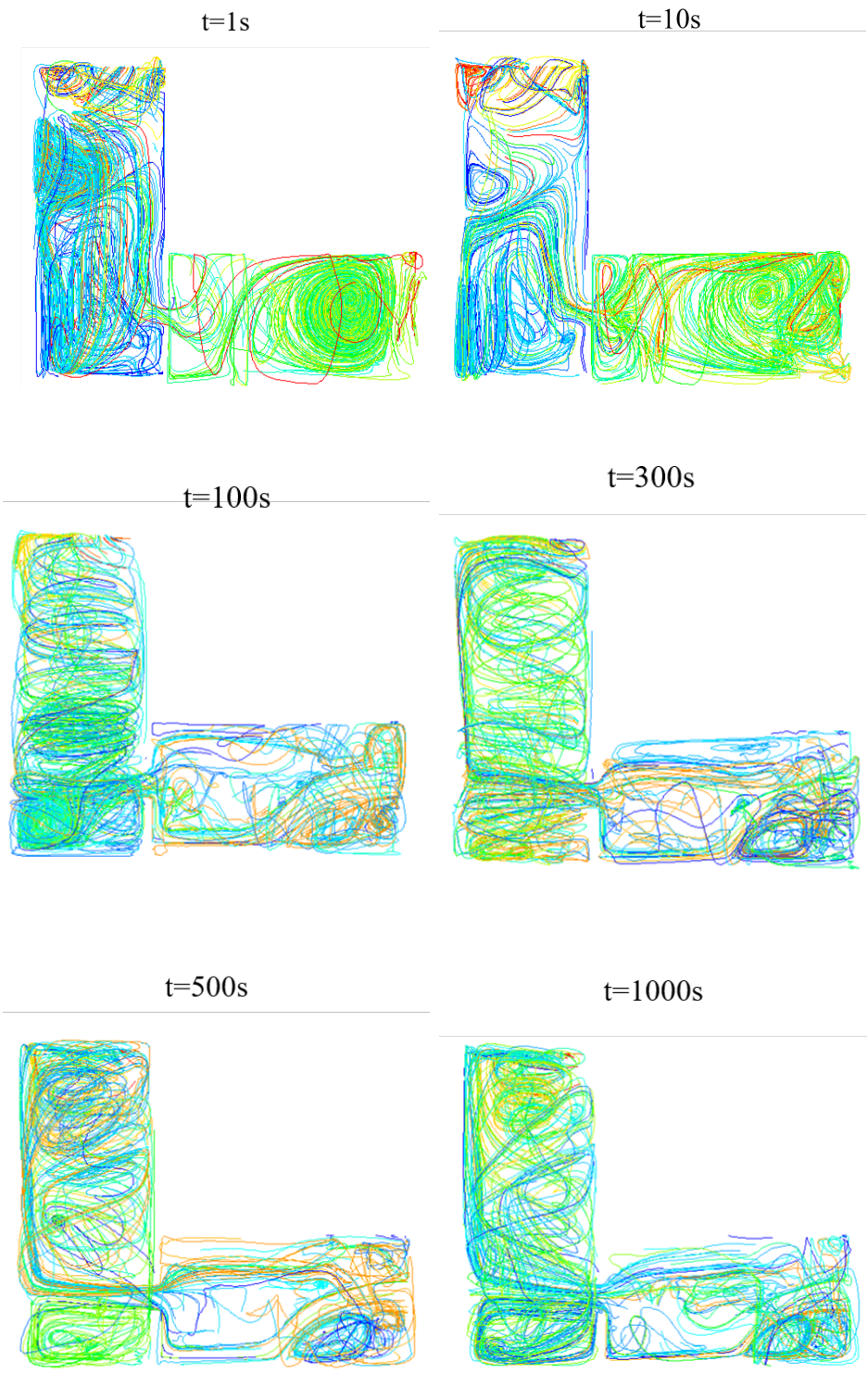

Figure 2-6: Plots of streamlines in the atrium building with a large heater(case A) at t=1, 10, 100, 300, 500, and 1000 s at the vertical measuring plane.

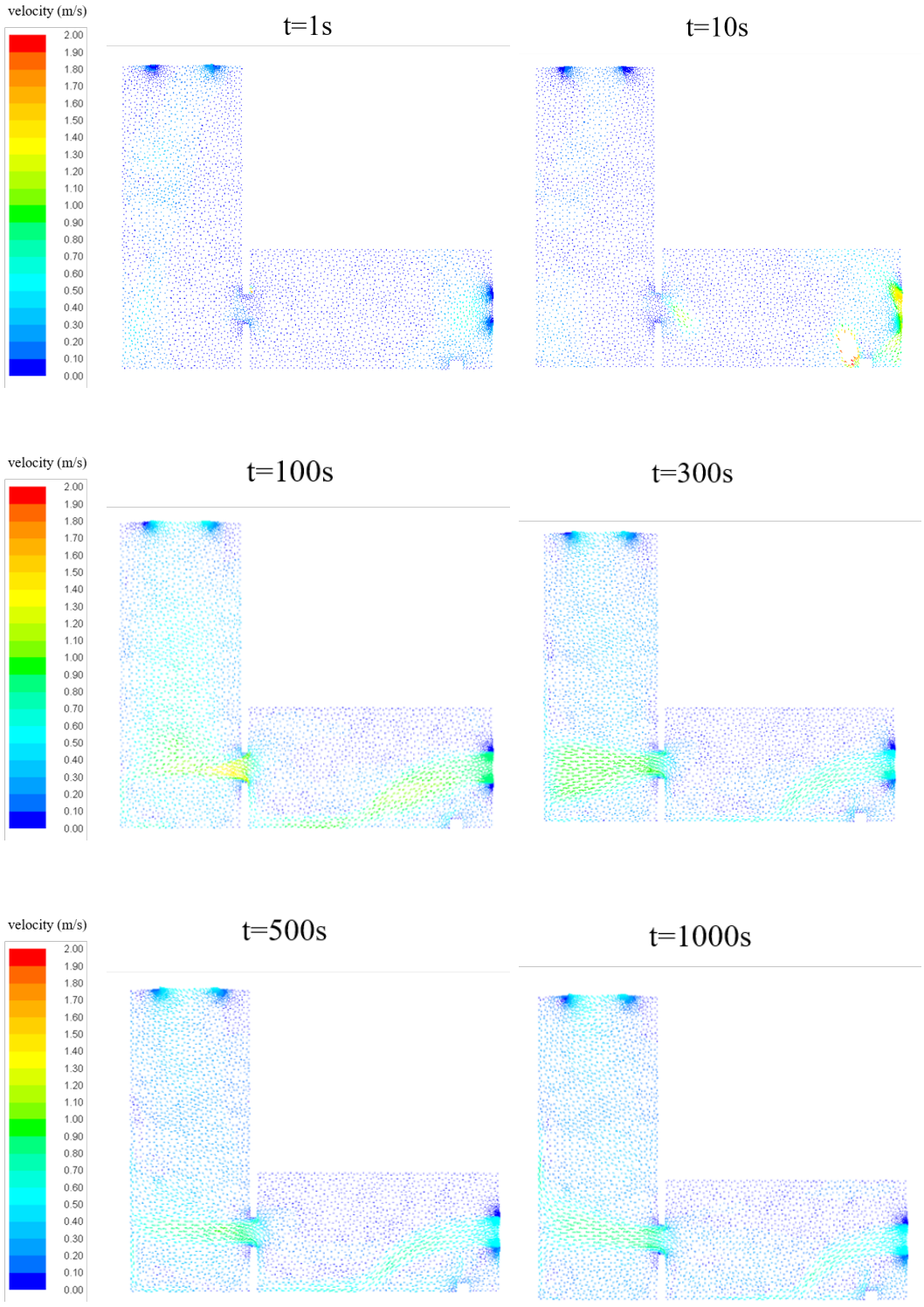

Figure 2-7: Vector plots of indoor air velocities of in the atrium building with a large heater(case A) at t=1, 10, 100, 300, 500, and 1000 s at the vertical measuring plane.

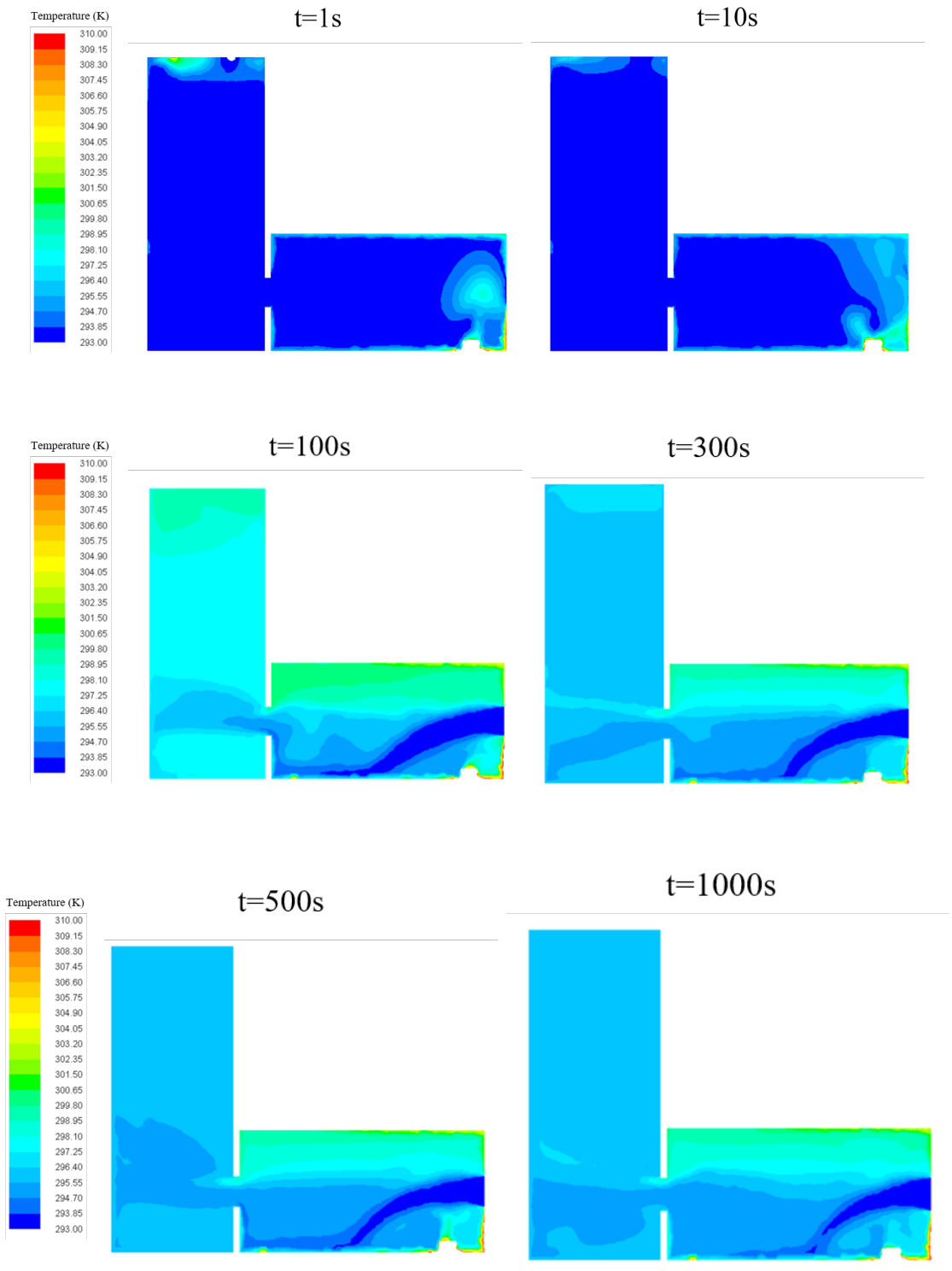

Figure 2-8: Contour plots of indoor air temperatures of in the atrium building with a large heater(case A) at t=1, 10, 100, 300, 500, and 1000 s at the vertical measuring plane.

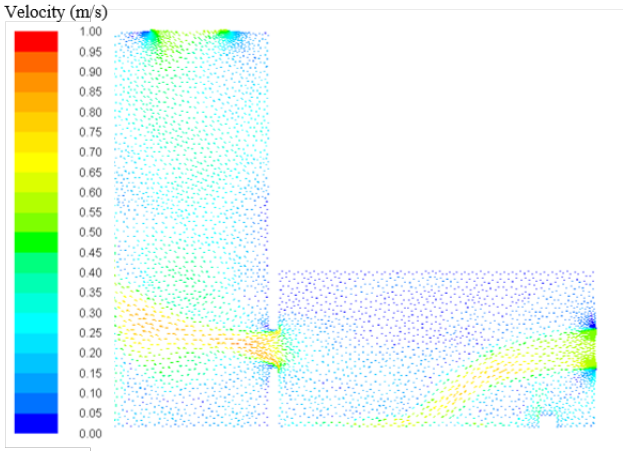

(a) The model with a large heater(1.68kW) near the sidewall(case A).

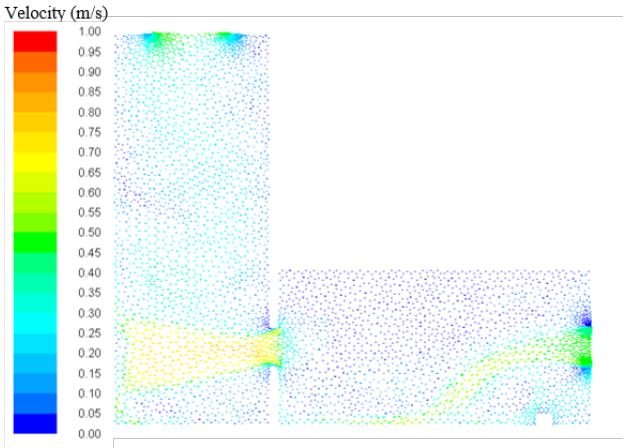

(b) The model with a small heater(1.12kW) near the sidewall(case B).

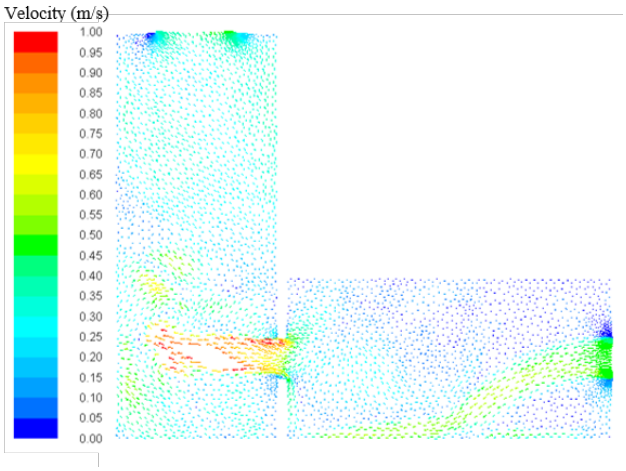

(c) The model with uniformly distributed heat flux($30W/m^2$) on the floor(case C).

Figure 2-9: Vector plots of indoor air velocities of case A, B and C at steady states at the vertical measuring plane.

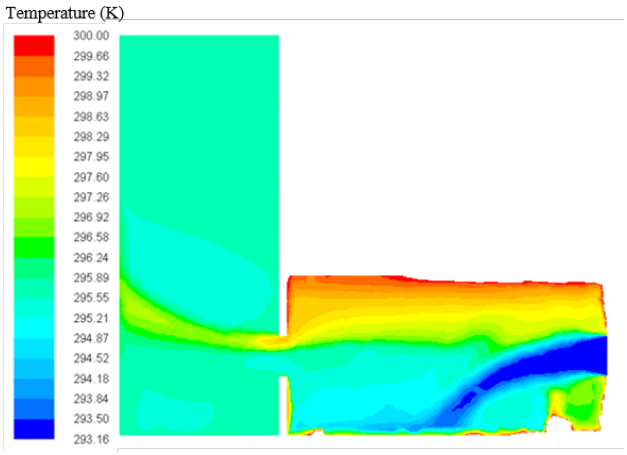

(a) The model with a large heater(1.68kW) near the sidewall(case A).

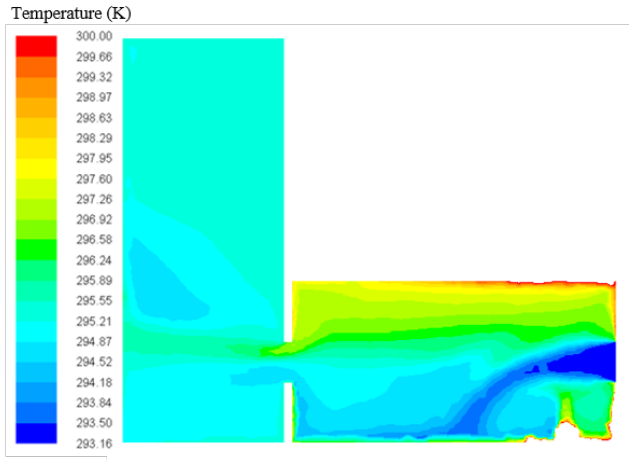

(b) The model with a small heater(1.12kW) near the sidewall(case B).

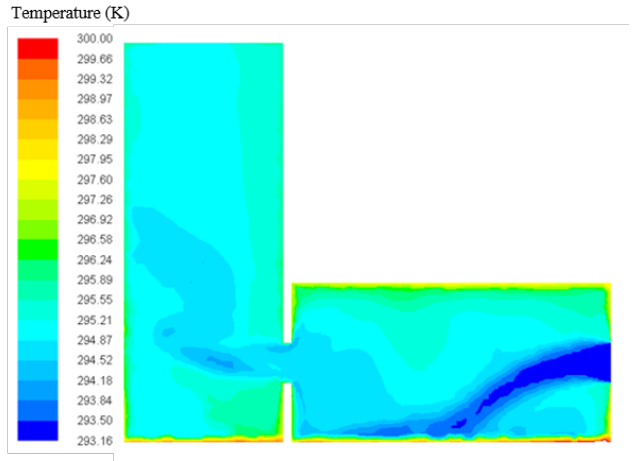

(c) The model with uniformly distributed heat flux($30W/m^2$) on the floor(case C).

Figure 2-10: Contour plots of indoor air temperatures of case A, B and C at steady states at the vertical measuring plane.

Fig.2-11 shows the velocity vector plots of cases with different opening locations at the top of the atrium. In cases with the same connecting window, air comes from the inlet on the sidewall, hits the floor due to gravity, generates a plume outside the connecting window, finally floats up and goes out through the top outlet. Differences between these cases are the flow features at the top outlet. The air flow at the middle outlet is a combination of two subflows, while flow at the south outlet tilts to the south and flow at the north outlet tilts to the north. Velocities in the cases with the same floor-to-ceiling opening between the room and the atrium are lower and steadier than those in cases with connecting windows, except the flow from the inlet and outlet. The only difference between them is the location of the flow from the outlet.

Temperature contours taken from the middle vertical planes in cases with different opening locations are presented in Fig.2-12. Temperature fields in the cases with connecting windows have little differences. Because of the buoyancy effect, top hot air and bottom cold air divide the room into two layers, while the air temperatures in the atrium are uniform. In the cases with floor-to-ceiling openings, temperatures are mixed in the whole space without a temperature stratification. Temperature differences are similar between cases with different outlets. Therefore, we can neglect the influence of outlet locations on temperature differences. The connecting opening is the main factor influencing temperature distributions in the room.

Figure 2-13 shows the velocity vector fields at the middle planes of models with different outlet sizes. Similar to cases mentioned above, air comes from the inlet, drops onto the floor, goes through the connecting window, hit onto the atrium wall and finally floats up to the ambient. The model with a small outlet shows higher velocities at the outlet but lower flow rates compared with the model with a large outlet. And air from the small outlet flows directly upwards while the air from the large outlet does not flow in the completely vertical direction.

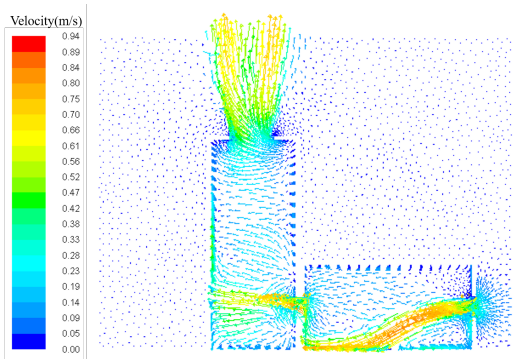

(a) The model with a middle outlet and a window connecting the room and atrium(case D).

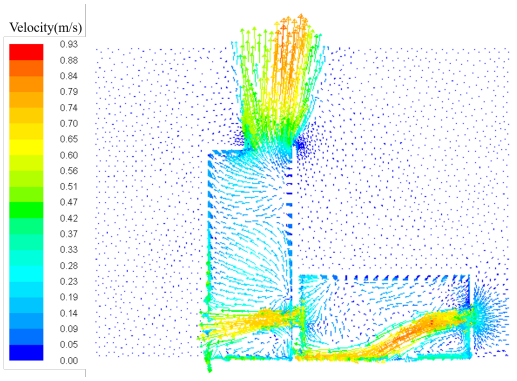

(b) The model with a south outlet and a window connecting the room and atrium(case E).

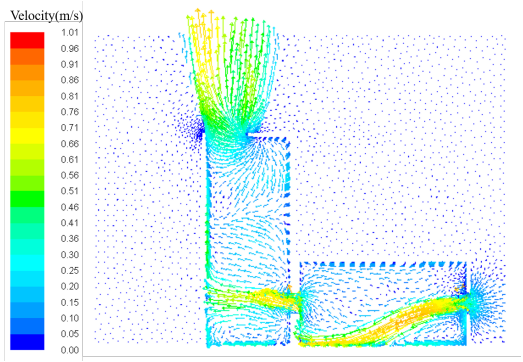

(c) The model with a north outlet and a window connecting the room and atrium(case F).

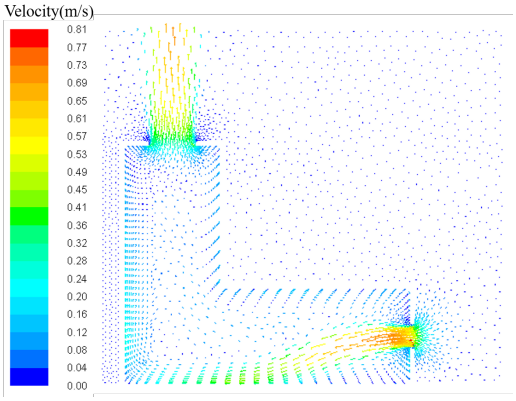

(d) The model with a middle outlet and a floor-to-ceiling connecting the room and atrium(case G).

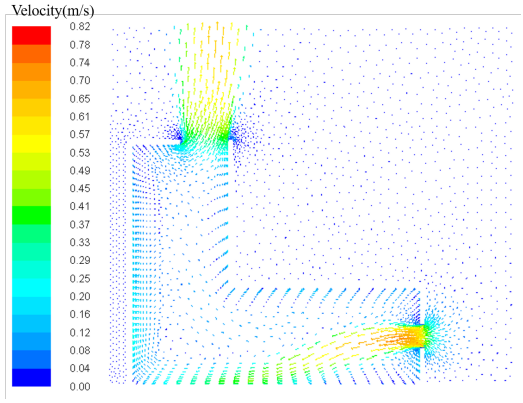

(e) The model with a south outlet and a floor-to-ceiling connecting the room and atrium(case H).

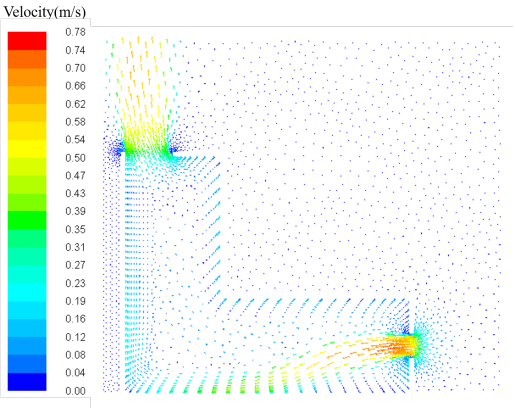

(f) The model with a north outlet and a floor-to-ceiling connecting the room and atrium(case I).

Figure 2-11: CFD predicted velocity vector plots taken from the middle vertical measuring plane of case D, E, F, G, H, I.

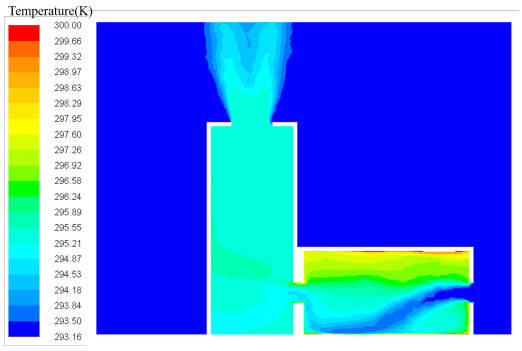

(a) The model with a middle outlet and a window connecting the room and atrium(case D).

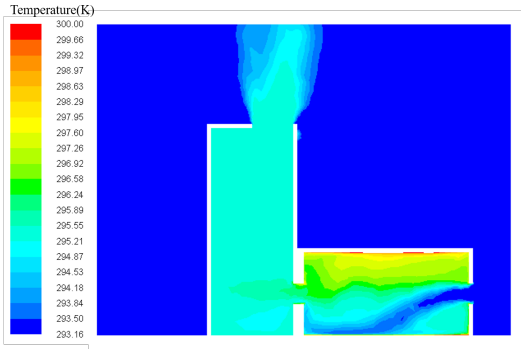

(b) The model with a south outlet and a window connecting the room and atrium(case E).

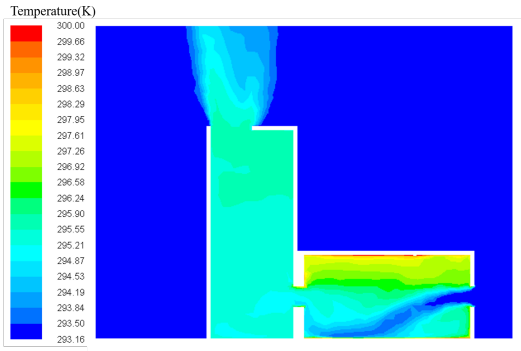

(c) The model with a north outlet and a window connecting the room and atrium(case F).

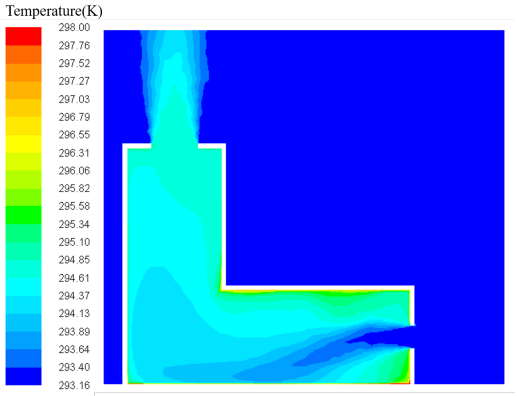

(d) The model with a middle outlet and a floor-to-ceiling connecting the room and atrium(case G).

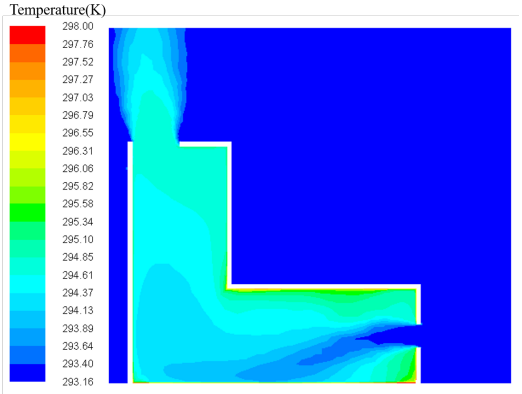

(e) The model with a north outlet and a floor-to-ceiling connecting the room and atrium(case H).

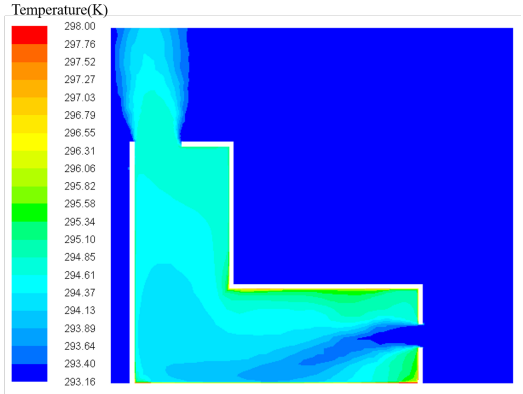

(f) The model with a north outlet and a floor-to-ceiling connecting the room and atrium(case I).

Figure 2-12: CFD predicted temperature contour plots taken from the middle vertical measuring plane of case D, E, F, G, H, I.

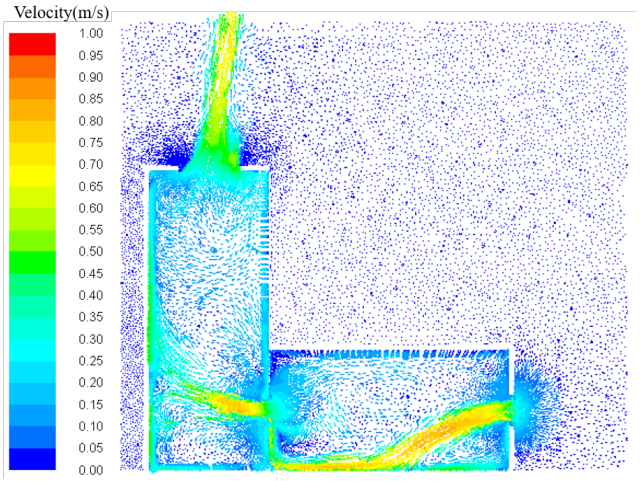

(a) The model with an original outlet(2m×2m)(case J).

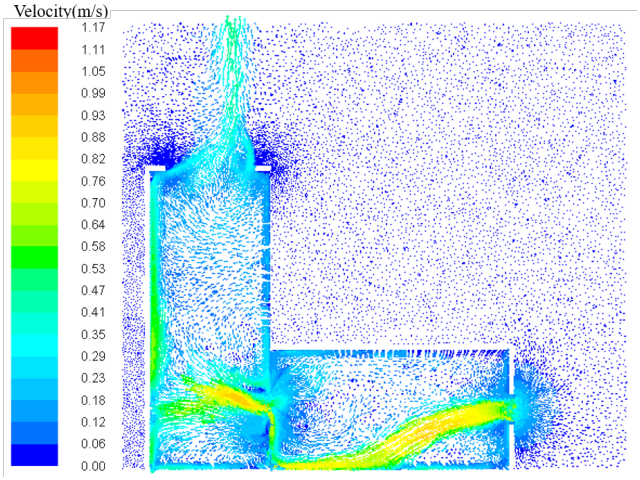

(b) The model with a large outlet(3m×3m)(case K).

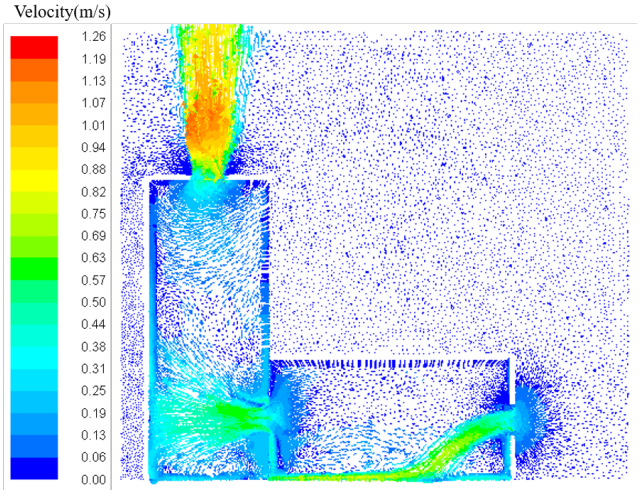

(c) The model with a large outlet(1m×1m)(case L).

Figure 2-13: CFD predicted velocity plots taken from the middle vertical measuring plane of models with different outlet sizes(case J,K,L).

Figure 2-14 shows the temperature contours at the middle planes of models with different outlet sizes. Temperature stratifications are obvious inside the rooms while there is more hot air on the upper layer in the model with a small outlet. There are not distinct plumes from the connecting windows which means the atrium zones are generally well-mixed. The model with a small outlet shows higher indoor temperatures while a large outlet leads to lower air temperatures in atrium.

The CFD investigations are compared to CoolVent[27], an airflow net work model adopted to capture the thermal environment and ventilation conditions. CoolVent combines the conservation of energy and momentum through numerical calculations. It assumes well-mixed conditions, applies negligible momentum among every zone[27]. All the building geometries, heat loads, and ambient conditions in the CFD models are used in CoolVent for comparison. Heat gains are uniformly distributed across floors in rooms.

Calculated air temperatures averaged over the volume of different zones from CFD and CoolVent simulations are provided in Table2.4 and 2.5. From the results in CFD models, air in the room reaches highest temperatures because of the heat gains from the floor. Bulk temperatures from the connecting window are lower than the average room temperature as a result of distinct temperature stratification in the room. The temperature difference between the initial ambient temperature and the final temperature from the top outlet is the highest in the model with a small outlet but lowest in the model with a large outlet. The main reason should be the different air exchange rates under different opening areas and resistance. Based on the well-mixed assumption, air temperatures in the room and atrium are uniform in CoolVent. The temperature increases from the inlet to the outlet are a little larger in CoolVent than the CFD models but are less than about 0.7K.

Calculated airflow rates at the inlets and outlets of the models in CFD and CoolVent simulations are shown in Table 2.6 and Table 2.7. According to the results in CFD models, flow rates leaving the top of the atrium to the ambient are lower than those from the ambient into the room. This results from calculating the average velocities for the imperfectly upward airflow from the outlet. The model with a large

outlet shows the highest flow rates while the model with a small outlet has the lowest flow rates, but the differences are smaller than 0.2kg/s. Calculated flow rates at inlets and outlets in CFD models and CoolVent models still match well with the differences less than 10%.

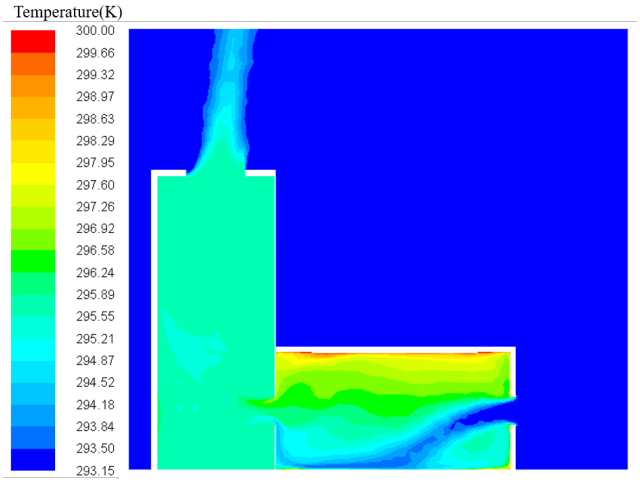

(a) The model with an original outlet(2m×2m)(case J).

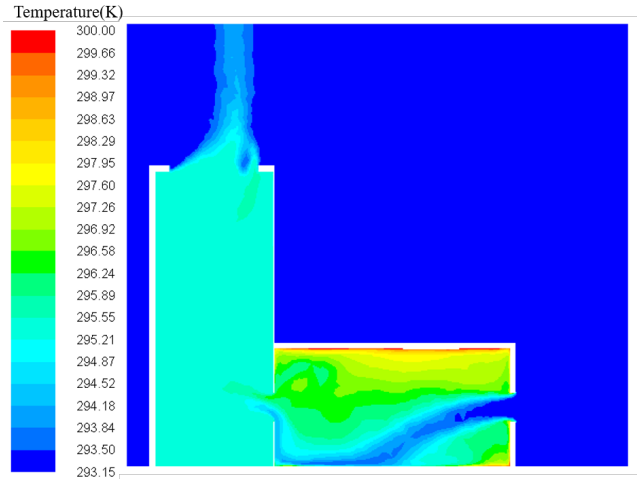

(b) The model with a large outlet(3m×3m)(case K).

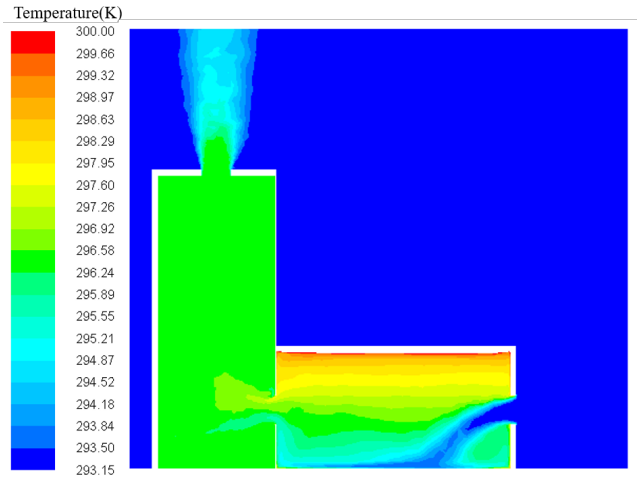

(c) The model with a large outlet(1m×1m)(case L).

Figure 2-14: CFD predicted temperature contour plots taken from the middle vertical measuring plane of models with different outlet sizes(case J,K,L).

Table 2.4: Simulated temperatures of different zones in buildings modeled with CFD.

Zone	CFD model	CFD model with a larger outlet	CFD model with a smaller outlet
Ambient temperature(K)	293.16	293.16	293.16
Room temperature(K)	295.98	296.02	296.87
Bulk temperature from the connecting window(K)	295.53	295.42	296.43
Atrium temperature(K)	295.98	295.45	296.46
Bulk temperature from the outlet(K)	295.50	295.45	296.47
Temperature increase from the inlet to outlet(K)	2.34	2.29	3.31

Table 2.5: Simulated temperatures of different zones in buildings modeled with CoolVent.

Zone	CoolVent	CoolVent with a larger outlet	CoolVent with a smaller outlet
Ambient temperature(K)	293.16	293.16	293.16
Room temperature(K)	295.97	295.94	296.51
Atrium temperature(K)	295.97	295.94	296.51
Temperature increase from the inlet to outlet(K)	2.81	2.78	3.35

Table 2.6: Simulated flow rates at the inlets and outlets in buildings modeled with CFD.

	CFD model	CFD model with a larger outlet	CFD model with a smaller outlet
Airflow rate from ambient(kg/s)	1.12	1.34	0.90
Airflow rate to ambient(kg/s)	1.13	1.21	0.86

Table 2.7: Simulated flow rates at the inlets and outlets in buildings modeled with CoolVent.

	CoolVent	CoolVent with a larger outlet	CoolVent with a smaller outlet
Airflow rate(kg/s)	1.01	1.03	0.85

Fig.2-15 shows the temperatures of different nodes in the CFD and CoolVent model versus height inside the atrium. Temperatures in atriumzone1 and atriumzone2 are uniform in the CoolVent model. But according to the CFD results, the large temperature change ranges at about 2m and 6.2m height are caused by the plumes from two connecting windows. And air temperatures in the lower half zone are relatively similar except those near the window while temperatures in the upper half zone increase with height. And Fig.2-16 gives the temperature and velocity plots at the middle plane of the two-storey model. Obviously, the plume from the second floor leads to the temperature stratification in the upper half of the atrium but the lower half are well-mixed. Furthermore, the upper layer causes higher indoor air temperatures in the room but lower velocities at the inlet and the connecting window.

Similarly, CoolVent simulations are applied for this special case by adding the number of floors in settings. Temperature and flow rate results obtained from two methods are shown in Table 2.8 and Table 2.9. Obviously, there is a disagreement in the airflow calculation between the CFD and CoolVent models. Simply using the average air velocities at the cross sections of the inlet and outlet in CFD models may lead to errors, because there are more grids near walls but fewer in the middle of the openings in meshing, which emphasizes velocities near walls. Therefore, to solve this problem, velocities in CFD models are adjusted by the biharmonic spline interpolation and integral based on limited values at unevenly distributed grids. Fig.2-17, Fig.2-18 and Fig.2-19 show the scatter, contour and surface plots of velocities normal to the cross section of the inlets and outlet. The contour and surface plots show that air velocities at the middle are generally higher than those near edges of openings but reach many peaks. Specially, air velocities near the lower edge is higher than those

near the higher edge of the inlet on the second floor. The simulated air velocities at the openings in CFD models generate irregular surfaces which is different from the assumption of regular surfaces in most bulk velocity calculations and theories. The comparison among the CFD and Coolvent models is shown in Table 2.10 and Table 2.11. The adjusted air flow rates calculated from the interpolation method are larger than the originally average air flow rates at the openings in CFD models. Table 2.12 shows that calculated heat gains of air based on the temperature increase and the flow rates and the actual heat loads in CFD models and CoolVent models. The heat gains in CoolVent are the closest to the actual loads. And the adjusted CFD models also match well with a slight decrease less than 10%. The air heat gains based on the adjusted results match well with the floor heat loads, which means the adjusted results are more accurate according to the conservation of energy.

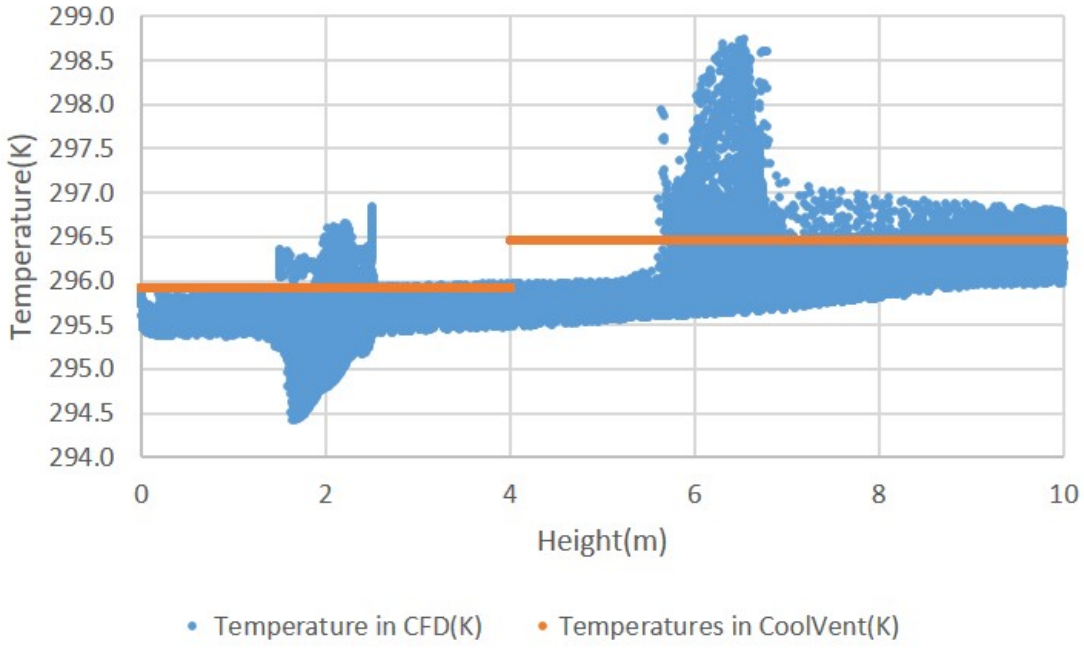

Figure 2-15: The scatter plot of air temperatures versus height inside the atrium of the two-storey model in CFD simulations and Coolvent.

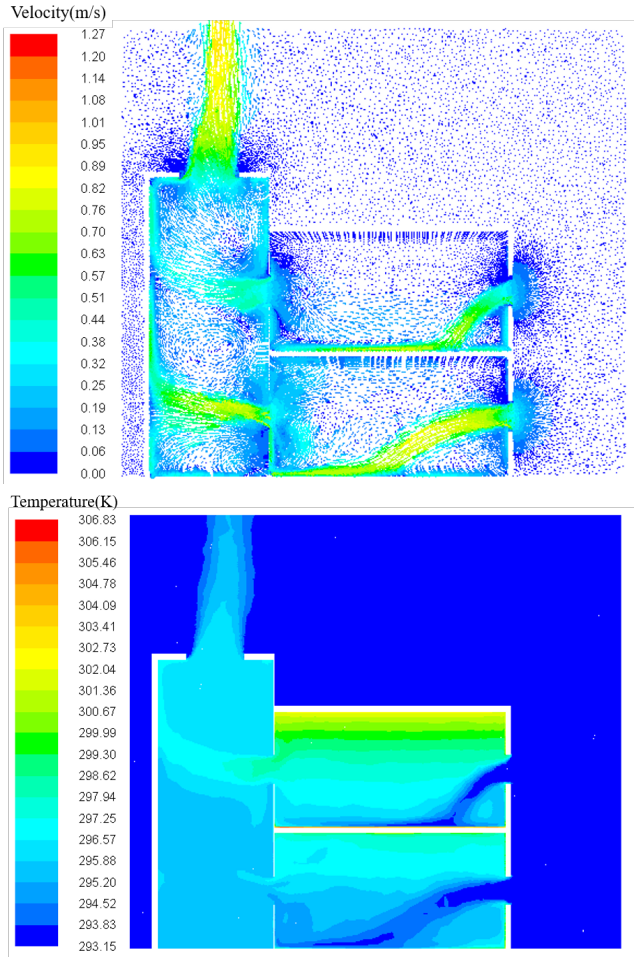

Figure 2-16: CFD predicted velocity and temperature plots taken from the middle vertical measuring plane of the two-storey model.

Table 2.8: Simulated temperatures of different zones in buildings modeled with CFD and CoolVent.

Zone	Temperature in CFD(K)	Temperature in CoolVent(K)
Ambient	293.16	293.16
Room1	295.94	295.92
Room2	297.61	297.26
Bulk temperature from the connecting window1	295.43	
Bulk temperature from the connecting window2	296.76	
atriumzone1	295.58	295.92
atriumzone2	296.14	296.46
Bulk temperature from the outlet	296.13	
Temperature increase from the inlet to outlet	2.97	3.3

Table 2.9: Simulated flow rates of different zones in buildings modeled with CFD and CoolVent.

	CFD model	CoolVent model
Airflow from inlet1(kg/s)	1.03	1.03
Airflow from inlet2(kg/s)	0.57	0.7
Airflow to ambient(kg/s)	1.62	1.73

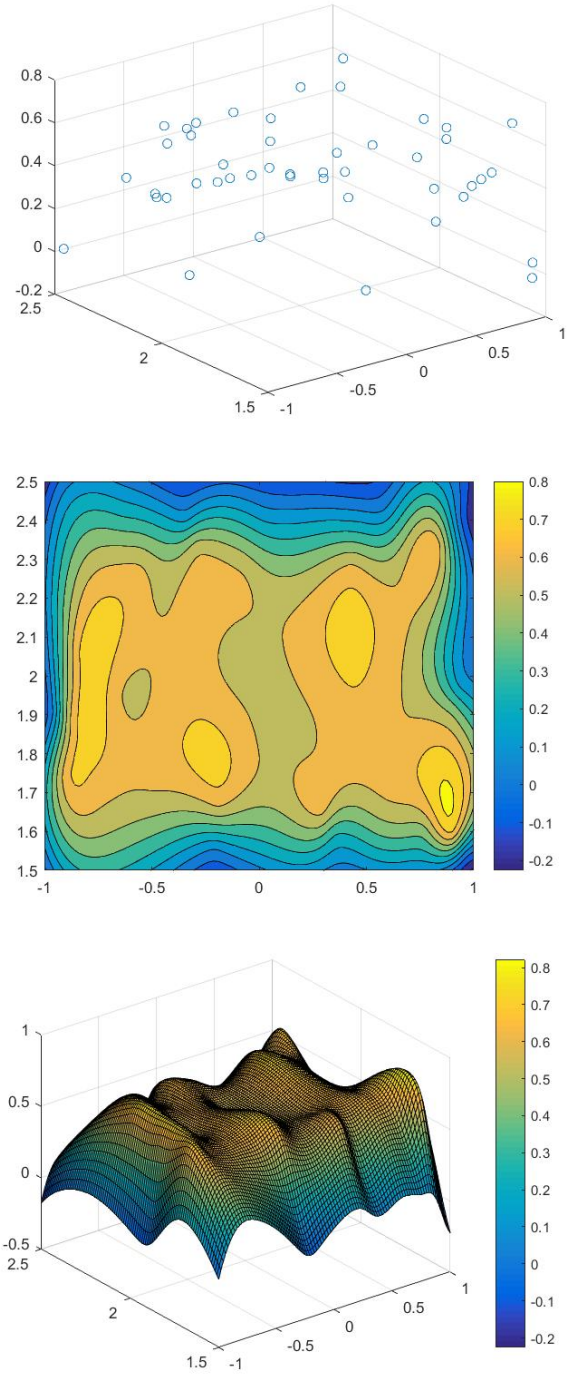

Figure 2-17: Scatter, contour and surface plots of air velocities taken from the cross section of the inlet on the first floor of the two-storey model.

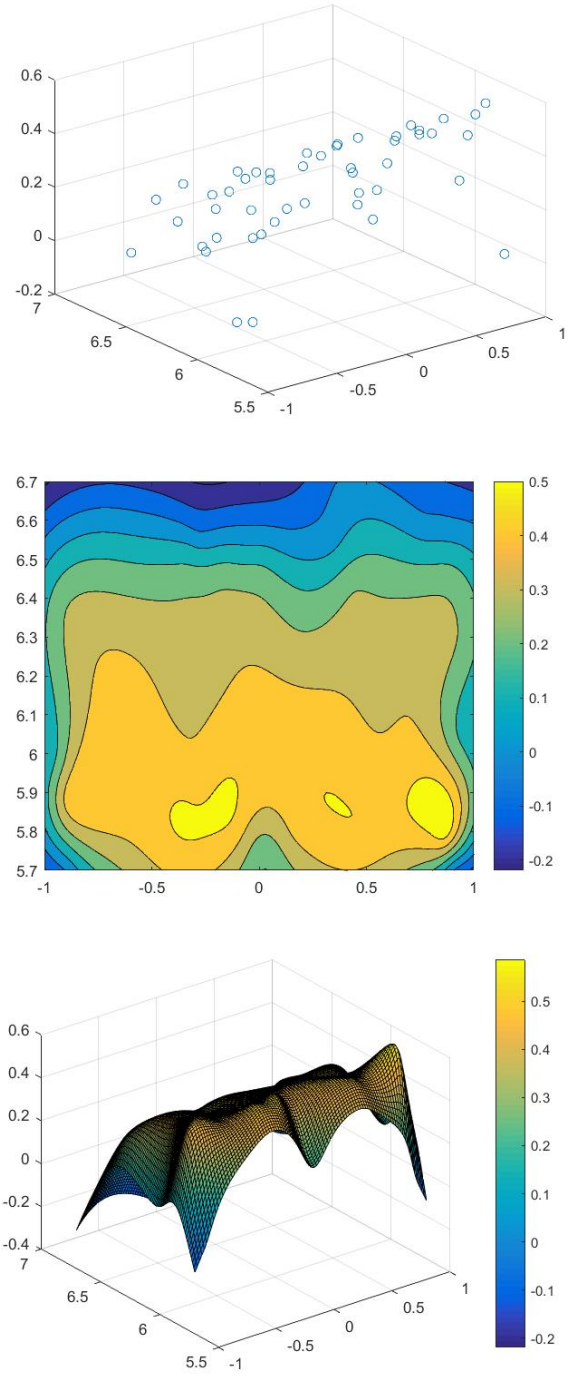

Figure 2-18: Scatter, contour and surface plots of air velocities taken from the cross section of the inlet on the second floor of the two-storey model.

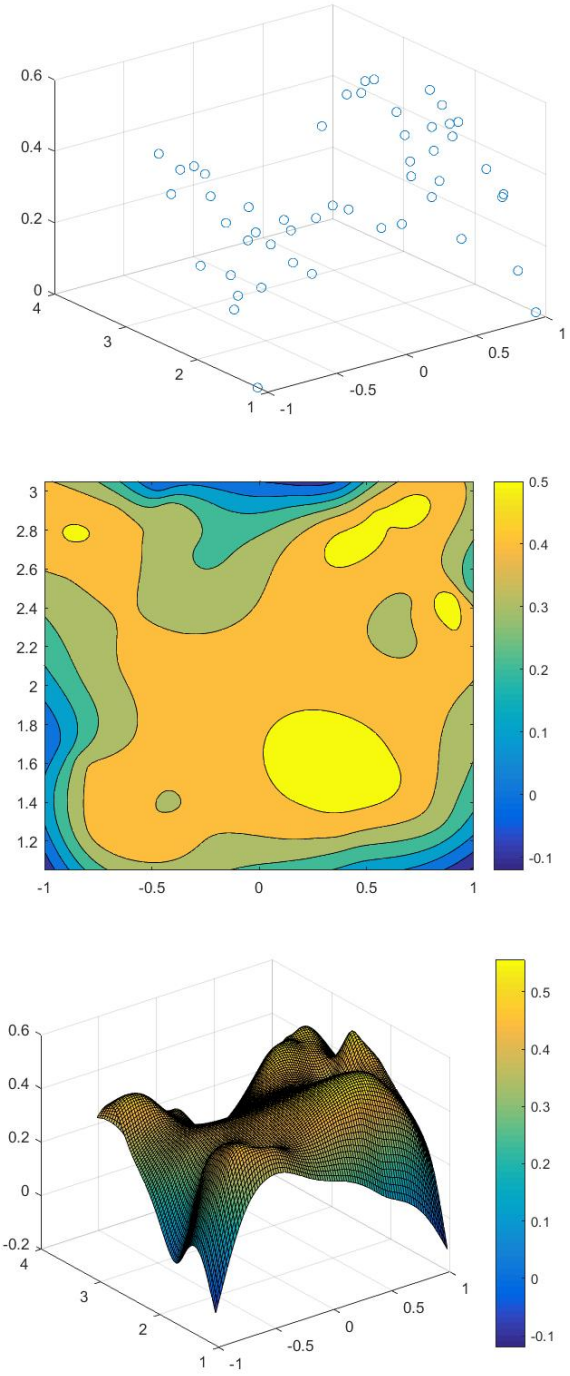

Figure 2-19: Scatter, contour and surface plots of air velocities taken from the cross section of the outlet of the two-storey model.

Table 2.10: Average air temperatures in CFD models, adjusted temperatures based on interpolation and integral in CFD models and simulated temperatures in CoolVent models of different zones in 2-layer buildings.

Zone	Temperature in CFD(K)	Adjusted temperature in CFD(K)	Temperature in CoolVent(K)
Ambient	293.16	293.16	293.16
Room1	295.94	295.94	295.92
Room2	297.61	297.61	297.26
Bulk temperature from the connecting window1	295.43	295.49	
Bulk temperature from the connecting window2	296.76	296.99	
Atriumzone1	295.58	295.58	295.92
Atriumzone2	296.14	296.14	296.46
Bulk temperature from the outlet	296.13	296.11	
Temperature increase from the inlet to outlet	2.97	2.95	3.3

Table 2.11: Averaged flow rates in CFD models, adjusted flow rates based on interpolation and integral in CFD models and simulated flow rates in CoolVent models from the inlets and outlet in 2-layer buildings.

	CFD model	Adjusted CFD model	CoolVent model
Airflow from inlet1(kg/s)	1.03	1.15	1.03
Airflow from inlet2(kg/s)	0.57	0.71	0.7
Airflow to ambient(kg/s)	1.62	1.85	1.73

Table 2.12: Comparisons between actual total heat loads and the calculated air heat gains in the CFD models and the CoolVent model.

	CFD model	Adjusted CFD model	CoolVent model
Calculated heat gains (kW)(based on flowrates from inlets)	4.78	5.51	5.74
Calculated heat gains (kW)(based on flowrates from the outlet)	4.84	5.48	5.74
Heat loads(kW)	5.76	5.76	5.76

2.4 Conclusions

This study investigates and compares the velocity fields and temperature stratification of naturally ventilated atrium buildings with different heat sources and openings. CFD models are applied to the analysis of the transient flow behaviors and steady state solutions. All cases can reach steady conditions after 1000 seconds and exhibit turbulent flow conditions. The buoyancy effect drives air to come through the inlet on the sidewall of the room, flow through the connection opening between the atrium and the room, float up in the atrium and go out from the top outlet.

We can ignore the differences in flow rates and velocity fields with different heat sources. The uniformly distributed heat fluxes reflects heat loads in real life leading to more mixed temperature distribution in the room than heat sources near the sidewall and simplify the mesh in CFD models. Therefore, the uniformly distributed heat flux is used in other CFD simulations in this chapter.

Different locations of outlets on the top of the atrium have little influence on the velocity and temperature fields inside the buildings. The connecting windows lead to high flow rates, and obvious temperature stratification near the connecting openings. In contrast, the temperatures are better mixed and velocities are more steady in cases with the floor-ceiling openings.

Lager outlets lead to higher airflow rates while airflow rates are lower in an atrium building with a smaller outlet but all other settings are the same. Furthermore, there are more uncertainties of air flow directions from the top larger outlet. On the other hand, temperatures in both the room and atrium are lower in the building with a larger outlet due to better air exchange effects. But a well-mixed temperature field in the atrium zone can be concluded in all cases with different outlet sizes and locations. Comparing the results from CFD and CoolVent result, both temperatures in different zones and flow rates match well with differences less than 10%. Thus, applying the airflow net work model with the well-mixed temperature assumption in zones are suitable for the single-layer atrium building.

Adding the number of floors would enhance the overall ventilation effects. The two-storey building model shows higher airflow rates and temperature increase from the inlets to the outlet than those in the single-storey model. Air flow rates are lower but the room temperatures are higher on the upper floor, because the shorter vertical distance from the inlet to the outlet results in a smaller pressure difference. An obvious temperature stratification can be observed in the upper half of the atrium which results from the plume from the room on the upper floor. Therefore, the assumption of a well-mixed temperature field in the atrium is inapplicable for multi-layer buildings. The velocity calculation by simply averaging the velocity values at grids of the cross section of openings brings apparent errors since the grids are unevenly distributed in meshing. Interpolation and integral based on limited velocity values could help to obtain more accurate results.

Chapter 3

Full Scale Experimentation of Buoyancy-Driven Ventilation

This chapter shows the full scale experiment conducted at a MIT building to characterize the temperature distribution and airflow in a real stairwell space.

3.1 Motivation of full scale experimentation

Well designed atriums can help significantly save energy and provide suitable thermal indoor comfort in natural ventilation without any aid of mechanical equipment. Various simulation tools are used to ensure the design at the early stage. Computational fluid dynamics(CFD) has become the most popular and is used in about 70% of publications in ventilation simulations reviewed by Chen[30]. Gan and Riffat[31] used CFD models to simulate a 14.6 m tall and 205 m^2 atrium. They compared the airflow rate changes with various opening configurations but failed to provide any experimental verification of the CFD results. Ji and Cook[21] carried out CFD simulations to study the buoyancy-driven ventilation flows in a single-storey space connected to an atrium with and without ventilation openings at the bottom of the atrium. They compared the results with predictions of analytical models and simple small-scale experiments. Unfortunately, those studies cannot provide experimental validation for CFD simulations.

Some full scale experiments in atriums or similar large single-cell buildings have been conducted and compared with CFD models. Cheng et al.[32] from Concordia University conducted a series of full-scale measurements of hybrid ventilation in a 17-storey institutional building and whole-building simulations using a 15-zone detailed and a 5-zone simplified model. They also found that the variations of weather conditions and dynamic interactions with hybrid ventilation systems can be accounted by flow coefficients in the simplified model. But the results are measured when mechanical ventilation systems are open and cannot guide the design of purely natural ventilation. Ray et al.[33] used a full-scale naturally ventilated atrium to validate CFD turbulence models and introduced a new airflow visualization technique using buoyant helium bubbles. But this study showed an unexpected bulk downward flow in the atrium without further accurate explanations and measurement.

More full-scale experiments are needed to characterize the actual temperature distribution and airflow conditions. These data would be used to validate CFD models beyond analytical models and small-scale experiments.

3.2 Building description

Proper atrium buildings with both openings on the top and bottom are relatively rare. Measuring the temperatures and flow rates in a typical atrium building is also source intensive due to the large space and many uncontrolled influencing factors. A typical five-storey stairwell chosen in this study, which is similar to a small atrium space, is at the south-east corner of MIT Building 35 which is shown in Fig.3-1. A floor plan of the Building 35 is shown in Fig.3-2. The stairwell is 20 m tall, 3.5 m high and 6 m wide. North and east doors on each floor are connections to the corridors in Building 35 and to Building 37. Four 2.5 m wide and 3 m high fixed windows on the south provide natural lighting in the stairwell. No mechanical ventilated system is installed inside the space. Although corridors are connected to the stairwell on every floor, all connecting doors shown in Fig.3-3 were closed to avoid passersby and air exchange. Thus, only purely natural ventilation would be considered inside the

stairwell.

Figure 3-1: Photograph of the stairwell exterior in Building 35 at MIT used in the full scale experiment.

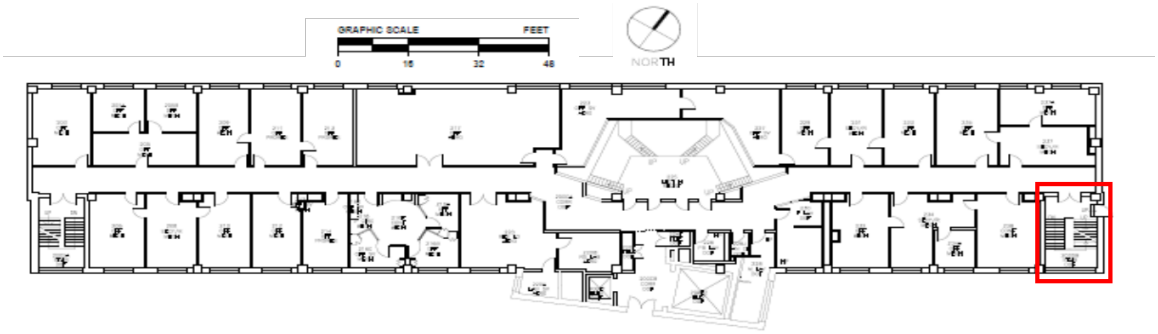

Figure 3-2: The floor plan of Building 35 with the stairwell in red box.

Figure 3-3: The photograph of the doors connecting corridors and the stairwell.

A south door on the ground floor was propped open to connect the stairwell and the ambient space. And also a west door on the top directly connecting to the roof was open. Both opening areas of the doors can be changed by adjusting the opening angles. Doorways are shown in Fig.3-4 All other door in the stairwell were closed and were labeled experiment notices during the process. Sunlight through south windows primarily heated the inner surfaces including walls, windows and stairs. The heating power was determined by the level of solar radiation and solar angles.

3.3 Instrumentation

The temperature distribution and airflow within the stairwell are characterized by the temperature measurement of indoor air on every floor and the air velocities measured at the ground door and roof door.

The thermometers used in this experiment are HOBO UX100-003 Temperature/Relative Humidity data loggers shown in Fig.3-5 produced by OnsetThe loggers can record temperature(Range: -20℃to 70℃Accuracy: ±0.21℃from 0℃to 50℃) and relative humidity (Range: 15% to 95% Accuracy: ±3.5% from 25% to 85%) in indoor environments with its integrated sensors. To test the air temperatures at the middle space and avoid disturbance from other surfaces, ten temperature sensors equally dividing

Figure 3-4: Photographs of two openings connecting the stairwell and ambient. A bottom door(left) on the ground floor is open during the experiment and a top door(right) leading to the roof is left open.

the whole zone into 10 small zones in the vertical direction hung from the railings. Locations of thermometers are shown in Fig.3-6. Ambient temperatures are measured by a thermometer located outside the bottom door. Because surface temperatures are difficult to measure using HOBO, an infrared thermometer(Range: -20℃to 315℃) produce by RYOBI[34] was used to detect hot and cold spots near walls and windows, which is shown in Fig.3-7

Figure 3-5: The thermometers measuring air temperatures in the experiment.

Figure 3-6: Locations of the thermometers when hanging from the railings. Red dots represent thermometers.

Figure 3-7: The infrared thermometer measuring surface temperatures in the experiment.

Velocities are measured at the bottom door on the ground floor and the top door connecting to the roof to get volumetric flow rates. The measurement are taken at 12 points at the openings using the equal area method for the entrance to a rectangular duct according to ASHRAE Standard 111-2008. Two Graywolf AS-201 hotwire anemometers which have the accuracy of $+/-3\%$ are used. Because the velocities fluctuate rapidly due to wind fluctuation, only relatively average values estimated by testers in short time periods are recorded. Volumetric flow rates are calculated by multiplying average velocities and opening areas.

3.4 Experimental procedure

This field experiment was conducted from 9:50 am to 11:00 am on Sunday, April 30,2017 at the stairwell of MIT Building 35. A Sunday was chosen to reduce the impacts of occupants. Solar gains in the daytime experiment assisted the buoyancy effect. Testers monitored the doors during the whole process to prevent any safety problem. All doors connecting corridors were closed from 9:50. To observe the effects of different opening sizes, the bottom and top doors were fully open from 9:50 to 10:30 but half open from 10:30 to 11:00 by adjusting the opening angle from 90°to 45°. The opening areas of the two doors are different, which are shown in Table 3.1. Temperatures were logged at a sampling rate of 1 min to catch the real-time change, while the velocities were tested every 10 minutes(9:50, 10:00,10:10, 10:20, 10:30, 10:40, 10:50, 11:00). To study the influence of inside surfaces, all surfaces including walls in four sides, stairs, windows are measured using the infrared thermometer.

Table 3.1: Areas of the bottom and top doors at different opening conditions.

	Bottom door	Top door
Fully open area(m^2)	2	3
Half open area(m^2)	1	3

3.5 Results

Fig.3-8 shows the outside velocities measured at the outside ground near the bottom door every ten minutes during the experiment process. The thermometer was placed two meters away from the bottom door and 1 meter high. Outside wind velocities changed but kept below 1 m/s in most time. The direction of the outside wind remained from east to west. Flow rates at doors are shown in Fig.3-9. Because the velocities always fluctuated rapidly when measuring, the recorded values contain measuring errors. The flow rates at the top door are lower and more stable than those at the bottom door. After the doors became half open, the flow rates at the top door decreased but the rates at the bottom door failed to show similar change. Based on

the conservation of mass of air inside the stairwell, the measurement at the bottom door is inaccurate. The decrease of flow rates at the top door is more than half when the opening area of the doors were adjusted to a half.

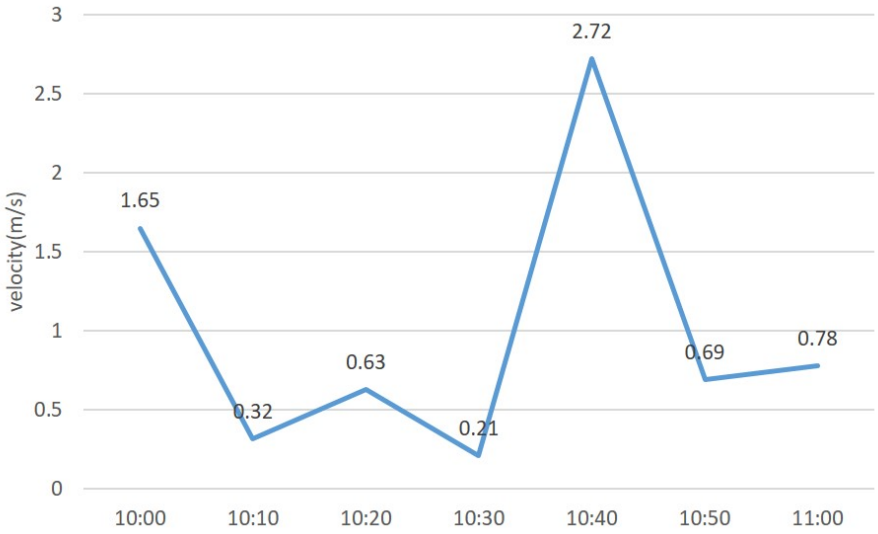

Figure 3-8: Outside velocities measured every ten minutes at the outside ground.

Figure 3-9: Flow rates calculated by measured velocities every ten minutes at the bottom and top doors.

Fig.3-10 shows the measured surface temperatures of east wall, south wall, west wall, north wall, stairs and windows. Temperatures of windows are obviously about

4 degrees lower than temperatures of other surfaces, because the overall heat transfer coefficient of the glass is much higher than that of others leading to surface temperatures closer to the ambient air temperatures. But temperature differences among the walls and stair are relatively small at every time. A decline from 9:50 to 10:30 and an uptrend from 10:30 to 11:00 reveal that the air flows passing though the surfaces cool them at the early stage but solar gains may heat them after 10:30.

Fig.3-11 shows the surface temperatures on different floors at 10:30. Temperatures gradually increase with the floors because air gains heat from surfaces inside during the process. An exception are temperature changes from fourth floor to fifth floor. Temperature discrepancies are small among walls in four sides, which may show good heat insulation.

Measured air temperatures of different floors and outside changing with time are shown in Fig.3-12. Outside temperatures fluctuate and increase from 14℃to 16.3℃due to the solar gains but rise an abnormal peak at 10:30 which may be influenced by an unknown temporary ambient heat source. Because the connecting doors on every floor were closed at 9:50 and the air exchanges were blocked, the air temperatures drop down from 9:50 to 10:00. Fluctuations of air temperatures during the experiment period on every floor are small after 10:00.

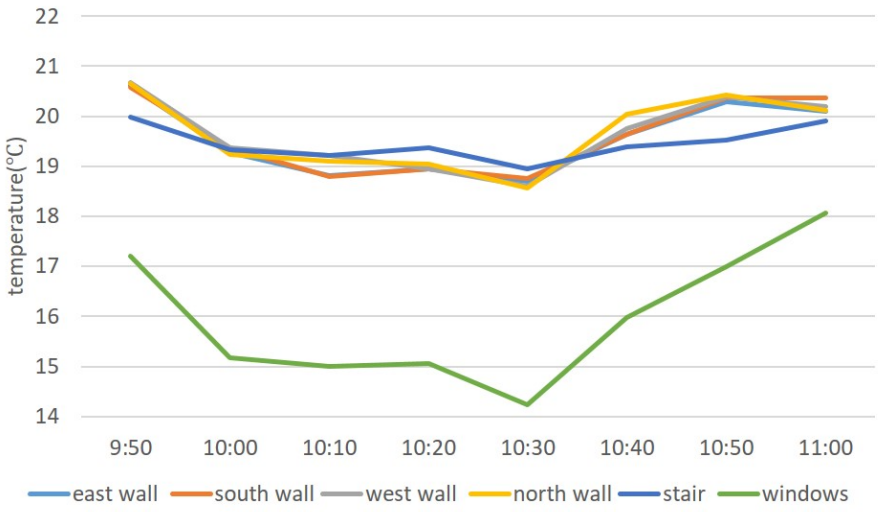

Figure 3-10: Surface temperatures averaged among different floors at various times during experiment.

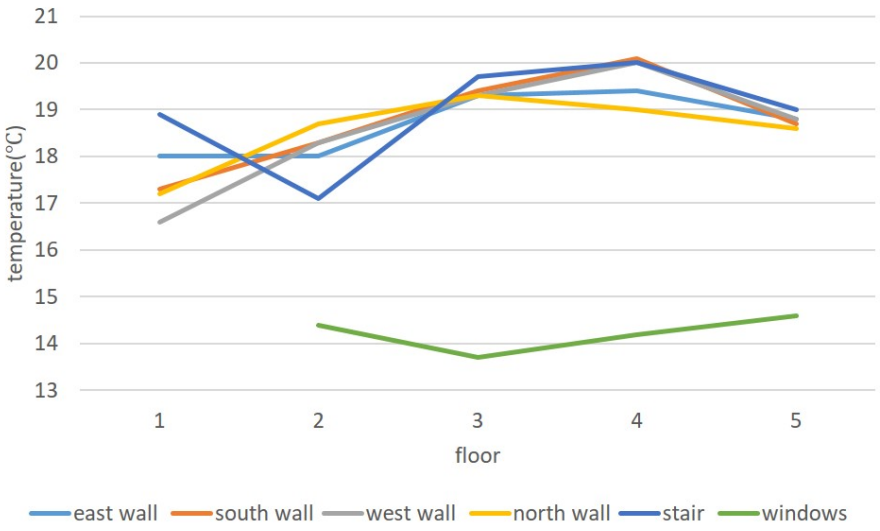

Figure 3-11: Surface temperatures measured at 10:30 on different floors.

Fig.3-13 reflects the measured air temperatures at different times versus different floors. Because air from ambient is heated by the inner surfaces on every floor, the temperatures increase at a comparatively stable rate versus the heights based on the stable slope of the curves after 10:00.

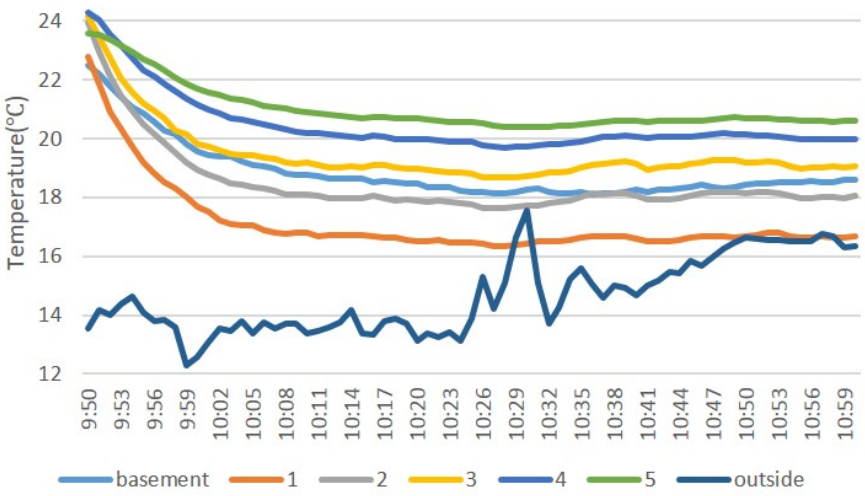

Figure 3-12: Air temperatures of different floors and outside changing with time.

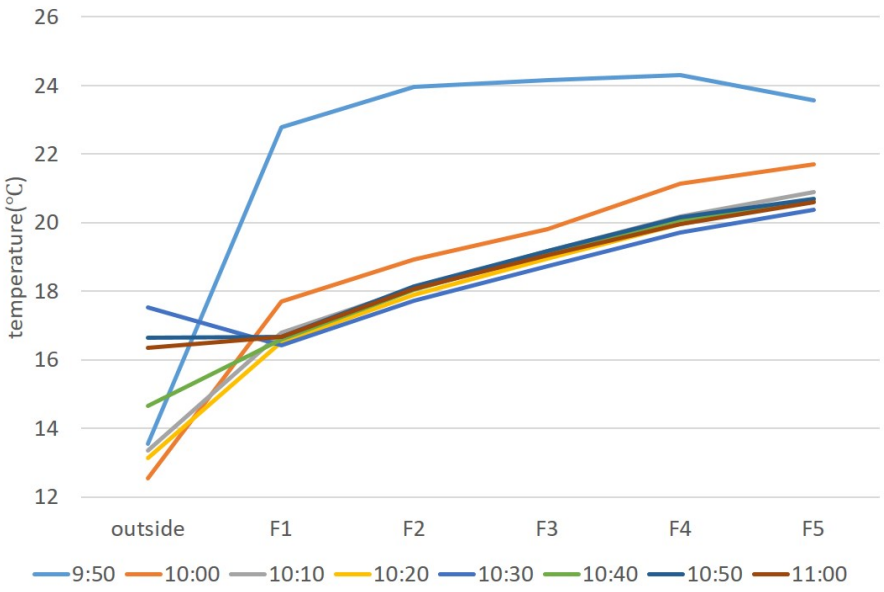

Figure 3-13: Air temperatures of different times changing with floor increase.

3.6 Conclusions

Experimental flow rates at the bottom and top doors fluctuate frequently and randomly which are not in phase and also not accurately consistent with the outside wind velocity change. The obstruction of surrounding buildings, volatile wind directions and the delay of the air flow process could be the main reasons. Surface temperatures of different walls and stairs are close but increase along with the height. The reason is that higher floors receive more solar gains than the lower floors in the shade from other buildings. Moreover, vertical indoor air temperature distribution would also influence the surfaces.

Indoor air temperatures on every floor are relatively stable during the experiment time. However, the air temperatures keep rising when flowing from the bottom to the top. That is the air gains heat from the hotter surfaces when blowing though them and then enhances the buoyancy effect. These results prove that the well-mixed conditions in the stairwell or atrium buildings used in many studies are unsuitable when the cross section areas are small. The gradually increasing temperature fields in the vertical direction inside atriums reflect real situations.

Chapter 4

Analysis of the Full Scale Experiment

4.1 Motivation of theoretical analysis and calculations

Recall the results from the full scale experiment in the previous chapter. Flow rates are decided by the buoyancy effects and the resistance of the inlet, outlet and passway. Air temperatures are affected by the surfaces temperatures, heat transfer efficiency and flow conditions. Thus, Flow rates and temperatures influence each other. Further investigations for the effects of those factors are still needed. This chapter analyzes the motion and heat transfer process of air in the full scale experiment in the previous chapter. More calculations are provided to validate the results and predict the flow rates and temperature distributions in future natural ventilation studies in atrium buildings.

4.2 Geometry of the flow channel

The five-storey stairwell can be equally divided to ten sections in the vertical direction. There are two sections for every floor. During the ventilation process, ambient air coming from the inlet goes up through the inclined sections of stairs and then exhausts from the top outlet. Table 4.1 provides the geometry of every section

of stairs.

Table 4.1: Geometry of a sections of stairs.

Length(m)	6.32
Width(m)	1.75
Hight(m)	4
Hydraulic diameter(m)	2.43
Number of steps	10
Horizontal width of one step(m)	0.28
Vertical height of one step(m)	0.2

4.3 Resistance of the flow process

Flow rates measured at the bottom door and top door with their average values are listed in Table 4.2. The average flow rates are used to estimate the bulk flow velocities inside the stairwell. Calculated Reynolds number is about 50000, which is much larger than 2300. Thus, the flows are in the turbulent region.

Table 4.2: Measured flow rates at doors and averages in m^3/s at different times.

Times	Top door	Bottom door	Average
9:50	2.62	2.96	2.79
10:00	1.72	4.21	2.96
10:10	1.72	1.28	1.50
10:20	1.70	4.71	3.21
10:30	1.73	2.63	2.18
10:40	1.03	2.18	1.60
10:50	1.35	3.62	2.48
11:00	1.18	1.46	1.32
Average	1.63	2.88	2.26

The air flow rates between two zones, $V_{orifice}$, is calculated by the orifice equation, which is an empirical model based on the conservation of mass, conservation of momentum, and experimentally pressure drop through an orifice:

$$V_{orifice} = \rho A C_D \sqrt{\frac{2\Delta P}{\rho}} \tag{4.1}$$

where A is the area of the orifice in m^2, ΔP is the static pressure drop through the opening in Pa, ρ is the density of fluid in kg/m^3, and C_D is the dimensionless discharge coefficient. C_D is an empirical value which varies in different geometry and flow conditions. Many cases and relationships for hydaulic resistance can be found in Idelchik's book[7], which defines a resistance coefficient ζ and calculates the total pressure drop based on a known bulk velocity.

$$\zeta = \frac{\Delta P}{\rho v^2/2} \tag{4.2}$$

where v is the stream velocity in m/s. This ζ is converted to the discharge coefficient C_D in the orifice equation by equating the static pressure loss in two equations.

$$\Delta P = \frac{1}{C_D^2}\frac{\rho v^2}{2} = \zeta \frac{\rho v^2}{2} \tag{4.3}$$

The relationship between C_D and ζ is:

$$C_D = \frac{1}{\sqrt{\zeta}} \tag{4.4}$$

The value of ζ for the bottom and top doors are calculated using relationships for the exhaust, single top-hinged flap and the intake, single top-hinged flap, shown in Fig.4-1 and Fig.4-2. The ratios of the lengths and widths listed in Table 4.3 are the main factors affecting resistance. Calculated values of ζ and corresponding C_D are shown in Table 4.4 and Table 4.5.

Intake, single top-hinged flap

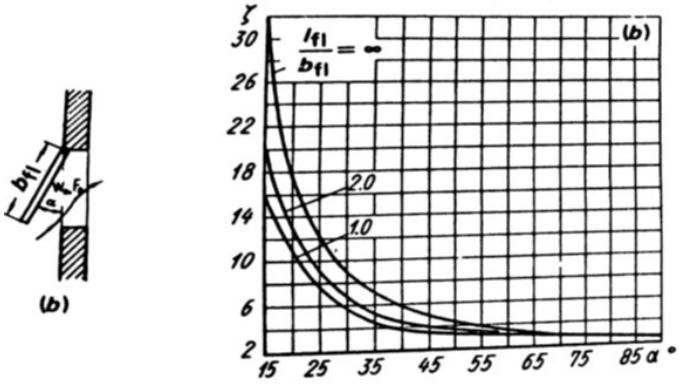

Values of ζ (graph b)

$\frac{l_n}{b_n}$	α, degrees						
	15	20	25	30	45	60	90
1.0	16	11	8.0	5.7	3.7	3.1	2.6
2.0	21	13	9.3	6.9	4.0	3.2	2.6
∞	31	18	12.5	9.2	5.2	3.5	2.6

Figure 4-1: Diagrams of resistance coefficients for intake, single top-hinged flaps.

Exhaust, single top-hinged flap

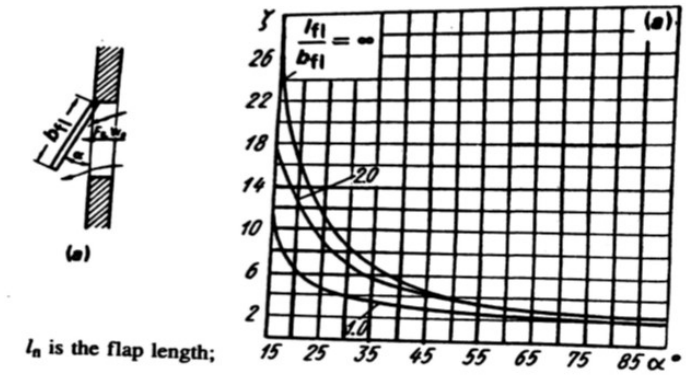

Values of ζ (graph a)

$\frac{l_n}{b_n}$	α, degrees						
	15	20	25	30	45	60	90
1.0	11	6.3	4.5	4.0	3.0	2.5	2.0
2.0	17	12	8.5	6.9	4.0	3.1	2.5
∞	30	16	11	8.6	4.7	3.3	2.5

l_n is the flap length;

$w_o = \frac{Q}{F_o}$; $\zeta = \frac{\Delta p}{\rho w_o^2/2}$

Figure 4-2: Diagrams of resistance coefficients for exhaust, single top-hinged flaps[7].

Table 4.3: The geometry of the bottom door and top door[7].

	Top door	Bottom door
length(m)	2	2
width(m)	1	1.5

Table 4.4: Values of ζ from Idelchik's Diagram 4-23 for exhaust, single top-hinged flap and intake, single top-hinged flap as shown in Figure 4-1 and Figure 4-2.

ζ	Top door	Bottom door
Fully open	2.5	2.6
Half open	4	3.8

Table 4.5: Values of C_D calculated based on the values of ζ in Table 4.4.

C_D	Top door	Bottom door
Fully open	0.6325	0.6202
Half open	0.5	0.513

The channel air passing through inside the stairwell can be modeled as many rectangular tube sections with smooth walls and walls of uniform roughness when considering the zigzag stair steps. Δ refers to the equivalent uniform roughness of walls, which is the height of every step. Fig.4-3 is the diagram of resistance coefficients for rectangular tubes.

$$\zeta = \frac{\Delta P}{\rho v^2/2} = \lambda_{non-c}\frac{1}{D_h} \tag{4.5}$$

$$\lambda_{non-c} = \frac{\Delta P}{(\rho v^2/2)(l/D_h)} = k_{non-c}\lambda \tag{4.6}$$

where D_h is the hydraulic diameters in m, and λ is friction coefficient determined as for circular tubes. The ratio of the length and width of the rectangular cross section decides the correction factor k_{non-c}. According to the values of geometry in Table 4.1, $k_{non-c} = k_{rec} = 1.05$, and relative roughness of walls $\Delta/D_h = 0.069$. For circular tube with walls of uniform roughness, the value of λ is 0.09 when Re is 10^5. Thus, ζ is 0.04. According to the air velocities through doors and inside the stairwell, the pressure drops are about 2.2Pa at the top door, 1.45Pa at the bottom door, and 0.156Pa though the stairwell. Thus, compared with the resistance of the inlet and outlet, the resistance of the stair sections can be ignored to simplify the calculations.

Tubes of rectangular, elliptical, and other types of cross section; stabilized flow.[87,158]

Diagram 2-6

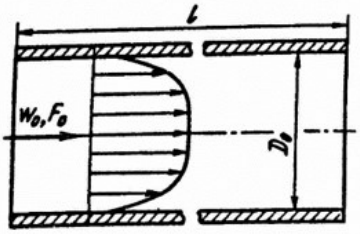

$$\zeta \equiv \frac{\Delta p}{\rho w_0^2/2} = \lambda_{non\text{-}c}\frac{1}{D_h}$$

$$D_h = \frac{4F_0}{\Pi_0} \quad Re = \frac{w_0 D_h}{\nu} \quad \lambda_{non\text{-}c} \equiv \frac{\Delta p}{(\rho w_0^2/2)(l/D_h)} = k_{non\text{-}c}\lambda$$

where λ is determined as for circular tubes from Diagrams 2-1 through 2-5

Shape of tube (conduit) cross section and schematic	Correction factor $k_{non\text{-}c}$						
	Laminar regime (Re < 2000, curve 1)						
	$\frac{b_0}{a_0}$	0	0.1	0.2	0.4	0.6	0.8	1.0
Rectangle:	$k_{non\text{-}c} = k_{rec}$	1.50	1.34	1.20	1.02	0.94	0.90	0.89
	Turbulent regime (Re > 2000, curve 2)							
	$k_{non\text{-}c} = k_{rec}$	1.10	1.08	1.06	1.04	1.02	1.01	1.0

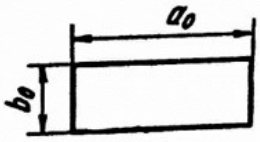

$$D_h = \frac{2a_0 b_0}{a_0 + b_0}$$

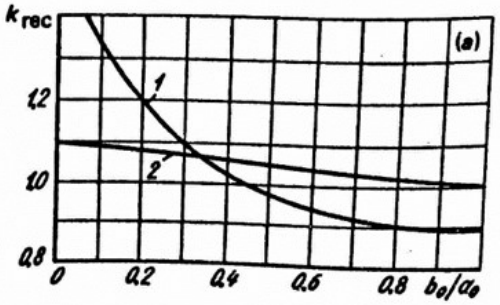

Figure 4-3: Diagrams of resistance coefficients for rectangular tubes[7].

4.4 Flow rates

During the experiment, indoor air is warmer than outdoor air because of internal heat gains. The density gradient inside is smaller than outside since warm air is less dense than cool air. The vertical distance between the lower inlet and the upper outlet is H. The hydrostatic pressure of air is decided by the density, height of air

column, and gravitational acceleration. Indoor and outdoor pressure gradients in a simplified buoyancy-driven ventilation model is shown in Fig.4-4. However, in real cases, the indoor pressure gradient is not a straight line but a curve determined by the temperature and density changes at different elevations.

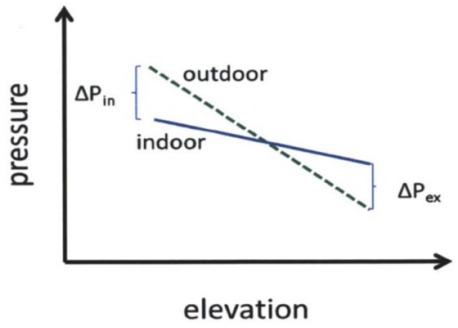

Figure 4-4: Indoor and outdoor pressure gradients versus elevation in simplified buoyancy-driven ventilation. The dashed line refers to the outdoor air assumed to be warmer than the indoor air while the solid line represents the indoor air.

The pressure drop among the flow channel can be ignored because the resistance is much less than resistance at doors. The difference of the outdoor and the indoor air pressure drives air coming from the ambient and exit from the top outlet, which is equal to the sum of the pressure drops at the bottom door and the top door:

$$\Delta P = \rho_{out} g H - \int_0^H \rho g dh = \Delta P_{bottom} + \Delta P_{top} \tag{4.7}$$

where the pressure drops at doors are calculated by $\Delta P = \frac{1}{C_D^2} \frac{\rho v^2}{2}$. The densities at different elevations are calculated based on the temperature distribution vertically.

4.5 Heat transfer coefficient

4.5.1 Convective heat transfer for smooth cases

The convective heat transfer process of air flowing through the walls in the stair sections is similar to heat transfer for fluid passing through smooth plates. The convective heat transfer coefficient, h, depends on many variables including flow geometry, surface roughness, flow velocity, viscosity and more. Dittus and Boelter[35]

gave the following correlation:

$$Nu = \frac{hD}{k} = 0.023 Re^{0.8} Pr^{n} \tag{4.8}$$

where D is the hydraulic diameter in m, k is thermal conductivity in W/mK, n is 0.4 for heating and 0.3 for cooling. Stanton, Reynolds and Prandtl numbers are evaluated by following fundamental formulae:

$$St = \frac{h}{\rho u c} \tag{4.9}$$

$$Re = \frac{\rho u D}{\mu} \tag{4.10}$$

$$Pr = \frac{c_p \mu}{k} \tag{4.11}$$

Combining and rearrange the equations, Stanton number for smooth cases is as follows:

$$St = \frac{Nu}{RePr} \tag{4.12}$$

4.5.2 Friction factor for ribbed cases

The roughness of the stair steps can be simplified as ribbed roughness on plates. An example of the ribbing configurations is shown in Fig.4-5, where p is the pitch and e is the rib height.

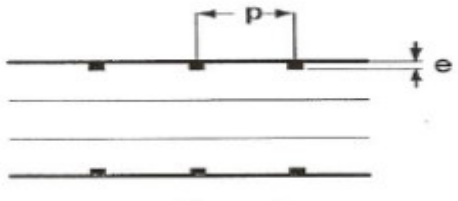

Figure 4-5: Convention for pitch and rib height in a pipe.

Nikuradse[36] recommended the "friction similarity law" for sand grain roughness by combining the velocity defect law and the law of wall. The roughness function

Re^+ is obtained by

$$Re^+(e^+) = (\frac{2}{f_r})^{0.5} + 2.5\ln(\frac{2e}{D_h}) + 3.75 \tag{4.13}$$

where f_r is the friction factor, and the roughness Reynolds number, e^+ is:

$$e^+ = \frac{e}{D_h} Re(\frac{f_r}{2})^{0.5} \tag{4.14}$$

Han[37] developed a correlation for the friction factor for turbulent flow between parallel plates with rib roughness by considering the geometrically non similar roughness p/e, rib shape angle Φ and the flow angle of attack α.

$$Re^+(e^+) = 4.9(\frac{e^+}{35})^m(\frac{10}{p/e})^{-n}(\frac{\Phi}{90^\circ})^{-1}(\frac{\alpha}{45^\circ})^{-0.57} \tag{4.15}$$

where m and n are given:

m=-0.4, if $e^+ < 35$; m=0, if $e^+ \geq 35$.

n=-0.13, if $p/e < 10$; n=$0.53(\frac{\alpha}{90^\circ})^{0.71}$, if $p/e \geq 10$.

Φ is 0, and α is 90°for stairs in the experiment.

4.5.3 Heat transfer for ribbed cases

Han[37] and Webb[38] gave the Stanton number in the ribbed flow:

$$St = \frac{f_r}{(He^+ - Re^+)(2f_r)^{0.5} + 2} \tag{4.16}$$

A correlation recommended by Webb[38] gives the values of He^+:

$$He^+ = 4.5(e^+)^{0.28}(Pr)^{0.57} \tag{4.17}$$

4.5.4 Consideration of mixed convection

Based on the measured flow rates in previous chapter, average Reynolds number is 51918 which is in the turbulent flow region. Because temperatures of walls and

stairs are higher than temperatures of air, buoyancy force can assist the forced flow. Thus, whether force or natural convection dominates heat transfer affects calculations of heat transfer coefficients.

The dimensionless group that characterizes a natural flow is the Grashof number which approximates the ratio of the buoyancy to viscous force on a fluid.

$$Gr = \frac{g\beta\Delta T D^3}{v^2} \tag{4.18}$$

where g is the acceleration due to Earth's gravity in m/s^2, β is the coefficient of thermal expansion, ΔT is the difference of the surface temperature and bulk temperature, D is the hydraulic diameter in m, and v is the kinematic viscosity in $kg/(ms)$. Estimated Gr is 2.13×10^9 according to experimental data. Gr/Re^2 is 0.79. The criteria for mixed convection in external flows when $Pr \leq 1$ are given in the following Table 4.6.

Table 4.6: Criteria for mixed convection in external flows.

Forced convection	$(Gr/Re^2) \ll 1$
Mixed convection	$(Gr/Re^2) \simeq 1$
Natural convection	$(Gr/Re^2) \gg 1$

Therefore, the heat transfer process is mixed convection.

For external natural convection of a flow on a vertical wall, Churchill and Usagi[39] defined a Prandtl number function Ψ as

$$\Psi = (1 + (\frac{0.492}{Pr})^{9/16})^{-16/9} \tag{4.19}$$

Churchill and Chu[40] correlated average Nusselt number for a turbulent flow as

$$Nu = 0.68 + 0.67(Ra\Psi)^{1/4}(1 + 1.6 \times 10^{-8} Ra\Psi)^{1/12}; 10^9 \leq Ra \leq 10^{12} \tag{4.20}$$

Churchill[41] recommended an appropriate correlation for mixed convection in external flows. For laminar or turbulent boundary layer flows with an assisting buoyancy

force on vertical plate, Nu is calculated by

$$(Nu - Nu_0)^3 = (Nu_f - Nu_0)^3 + (Nu_n - Nu_0)^3 \tag{4.21}$$

where subscripts f and n refer to forced and natural convection, and Nu_0 =0.

4.5.5 Heat balance

Outside air temperatures are known as the initial air temperatures. Air gains heat when flows though the surfaces inside the stairwell. The heat balance equation from energy conservation is

$$\rho u A C_p (T_b|_{x+\Delta x} - T_b|_x) = \Delta x h_i \Delta T_i P_i \tag{4.22}$$

where ρ is the density in kg/m^3, u is the bulk velocity in m/s, A is the cross section area in m^2, C_p is the specific heat in $kJ/(kgK)$, T_b is the bulk temperature in K, Δx is the flow distance in m, h_i is the heat transfer coefficient at surface i in $kJ/(m^2K)$, ΔT_i is the difference of the surface temperature and the bulk air temperature in K, and P_i is the perimeter in m.

When analyzing the heat transfer process, a machine room in the basement as shown in Fig.4-6 should be considered. Temperatures of the walls of the machine room are always much higher than indoor air temperatures. Some air from the ambient may flow down to the basement and be influenced by the heat loads from the machine room. This heat transfer process is so complex and uncertain that measured temperatures on the first floor are used in calculations.

Figure 4-6: Photographs of exterior and interior of the machine room in the basement.

All equations above are solved iteratively to calculate flow rates and temperatures by assuming an initial guess of flow rate is $1m^3/s$ and the initial indoor temperature is the ambient temperature. For every particular time, the ambient temperatures, indoor air temperatures on the first floor, all surface temperatures are known. The average of the temperatures at 10:20 and 10:40 is used as the temperature at 10:30 in calculations to revise the abnormal temperature peak at that time. Corresponding air temperatures are calculated though heat balance which leads to a new air flow rate. New heat transfer coefficients would be calculated using this new air flow rate. These iterations are performed until the change between the new and old flow rates is below 0.1%.

4.6 Results

Re, St, Nu, h and fr during the experiment calculated by iterations are shown in Table 4.7. Reynolds numbers change because of air velocity change and keep much larger than 2300, which are in the turbulent region. Nusselt numbers for the stairs are larger than those for the walls since the zigzag roughness enhances the heat transfer effects.

Table 4.7: Calculated Re, St, Nu, h and fr for stairs and walls during the experiment by iterations.

Time	Re	St	Nu_stairs	Nu_wall	h_stairs (W/m2K)	h_wall (W/m2K)	fr
9:50	80774	0.0029	484.68	168.11	5.35	1.86	0.56
10:00	70713	0.0027	422.26	151.14	4.66	1.67	0.54
10:10	62307	0.0026	381.70	136.61	4.21	1.51	0.51
10:20	60842	0.0026	374.27	134.04	4.13	1.48	0.51
10:30	44064	0.0026	300.20	103.57	3.31	1.14	0.45
10:40	40962	0.0025	284.41	97.70	3.14	1.08	0.43
10:50	33300	0.0025	249.32	82.79	2.75	0.91	0.40
11:00	32436	0.0021	229.58	81.20	2.53	0.90	0.39

The calculated air temperatures and measured air temperatures of different floors changing with time are shown in Fig.4-7. The outside air temperatures fluctuate with an upward trend and reach a peak at 10:30. These results of indoor air match fairly well. Both the calculated and measured air temperatures on every floor decrease form 9:50 to 10:00 but keep relatively stable from 10:00 to 11:00. Calculated temperatures of different elevations at the same time are lower than the actual temperatures. And the differences among different elevations of calculated temperatures are smaller than the those of actual temperatures during the process. Furthermore, calculated results shows a more obvious rising trend.

The comparisons of calculated air temperatures and measured air temperatures of different times versus floors are shown Fig.4-8. Air temperatures at 9:50 are higher than those at other times. The larger slope of the curves from the ambient to the first floor reflect a larger temperature rise because of influence of the basement. Measured temperatures keep higher than the calculated temperatures on every floor during the whole process. The calculated and measured temperature increases on every floor keep relatively steady with heights and time except 9:50. Moreover, the measured temperature increases on every floor keep larger than the calculated temperature

increases, which are caused by some unknown heats and unexpected errors in heat transfer coefficient calculations.

Measured flow rates and calculated flow rates at doors are shown in table 4.8 and Fig.4-10. Calculated values are in the range of flow rates at the top door and bottom door. However, their fluctuations are not in phase. Moreover, the calculated flow rates change to approximately one half when the opening areas are reduced by a half.

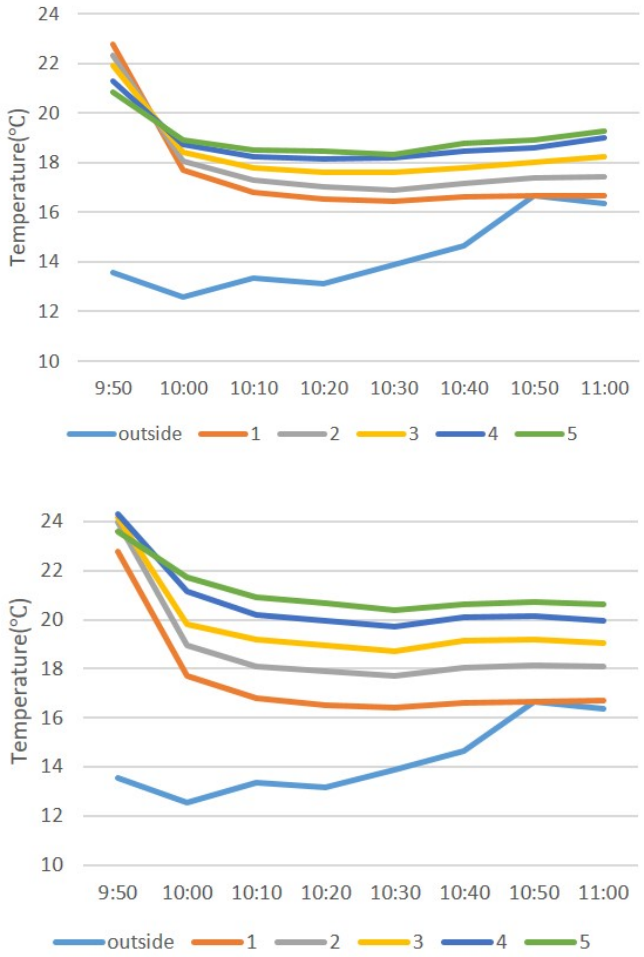

Figure 4-7: Calculated(up) and measured(below) air temperatures at different floors versus times.

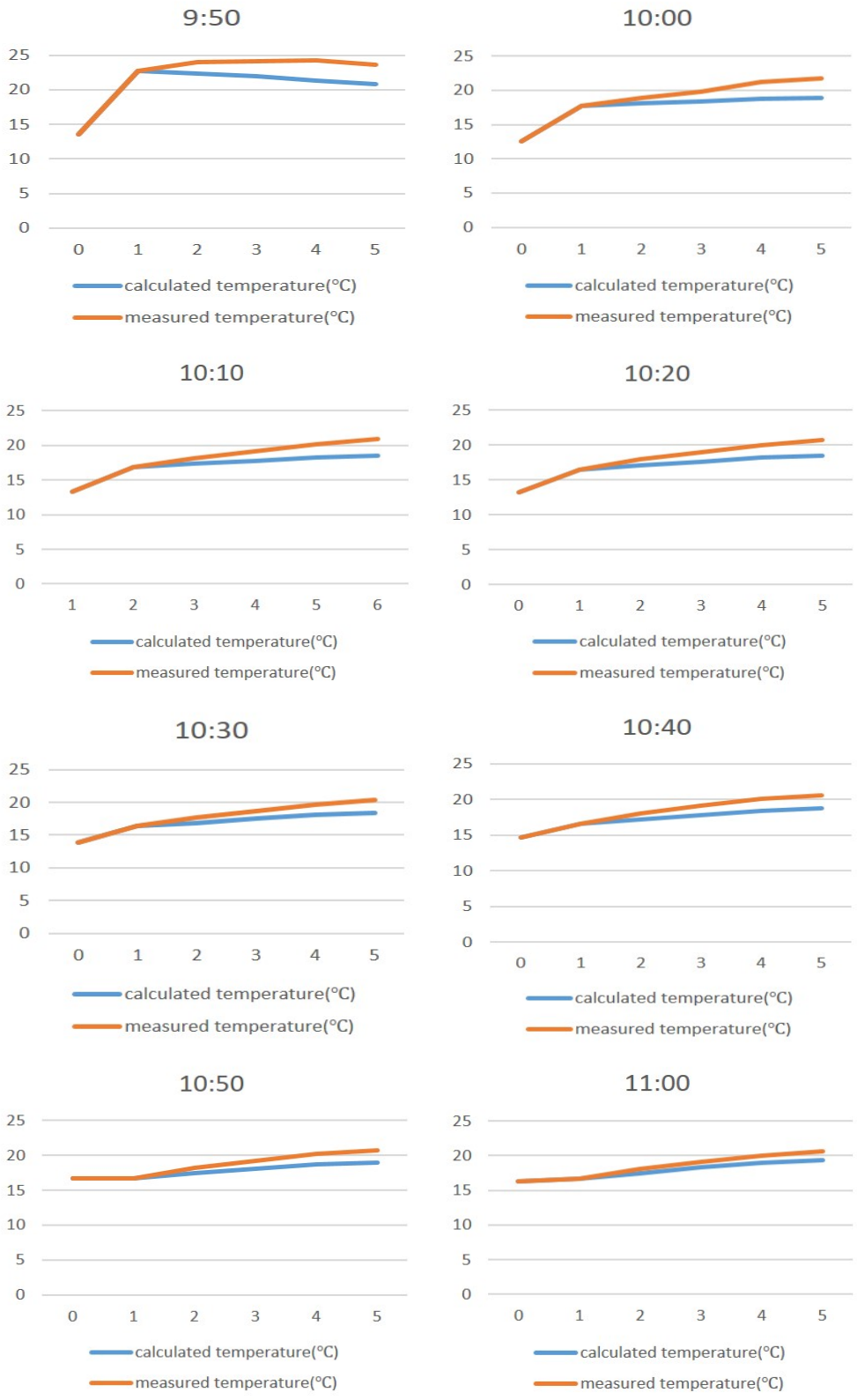

Figure 4-8: Calculated(blue curves) and measured(orange curves) air temperatures at different times versus floors.

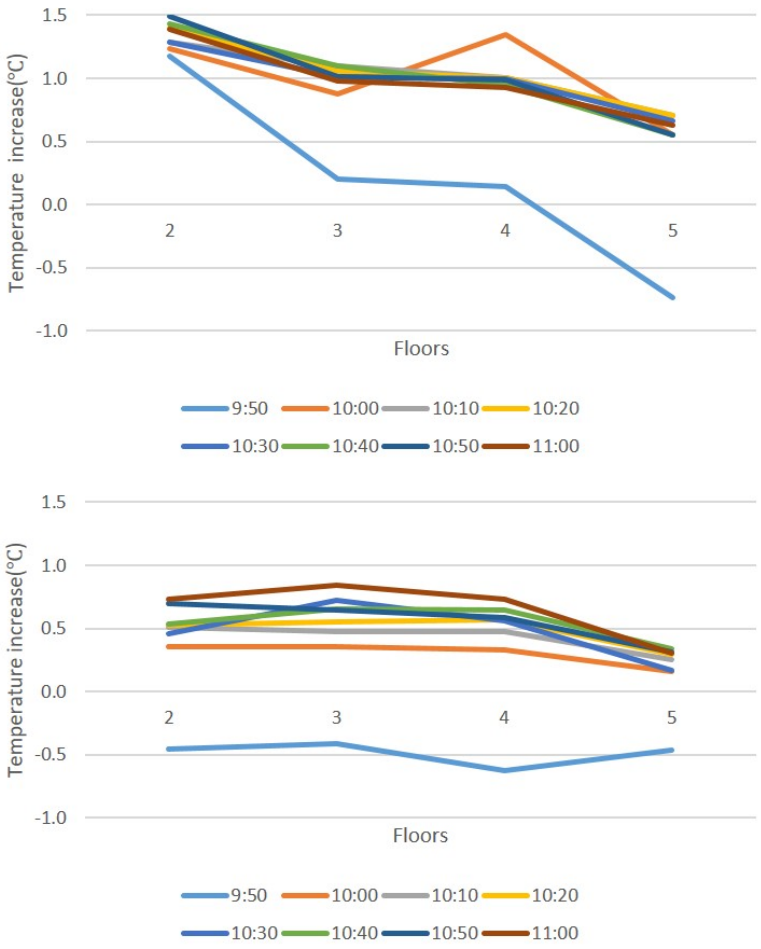

Figure 4-9: Measured(first) and calculated(second) air temperature increases at every floor at different times.

Table 4.8: Measured flow rates at top and bottom doors and calculated flow rates.

Time	Measured flow rates at top door(m^3/s)	Measured flow rates at bottom door(m^3/s)	Calculated flow rates(m^3/s)
9:50	2.62	2.96	3.41
10:00	1.72	4.21	2.88
10:10	1.72	1.28	2.52
10:20	1.70	4.71	2.53
10:30	1.73	2.63	1.83
10:40	1.03	2.18	1.71
10:50	1.35	3.62	1.10
11:00	1.18	1.46	1.31

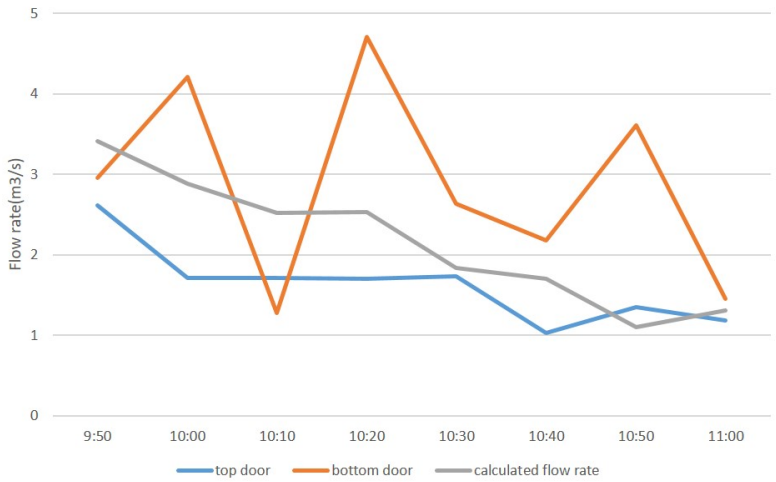

Figure 4-10: Measured flow rates at top and bottom doors and calculated flow rates versus times.

4.7 Conclusions

This chapter discusses methods to determine and calculate indoor air flow rates and temperatures inside a stairwell. Discharge coefficients of inlets and outlets are calculated from empirical equations based on the opening geometries. Pressure drops due to resistances of walls and stair steps can be ignored compared with pressure

change through openings in this experiment. Thus, indoor and outdoor pressure differences, which determine air flow rates, can be calculated with height difference and discharge coefficients.

Walls and stairs are considered separately as smooth plates and planes with ribbed roughness simply when calculating heat transfer coefficients. The height of roughness and distance between two stairs are main factors deciding enhancement of heat transfer. In addition, mixed convection should be considered by comparing Gr and Re^2. With known initial outside air temperatures, indoor air temperatures can be predicted by the heat gains of the air and the heat transfer processes at the surfaces.

Calculated results match well with the actual measured results in the previous chapter. Measured temperature increases on every floor are little larger than calculated temperature increases because of errors in the heat transfer coefficient estimation, especially the approximation of stairs as ribs. And the temperature increases keep relatively constant along with time. Calculated flow rates are about the mean values of flow rates at the top and bottom doors and change corresponding to the opening areas. However, fluctuations of air flow rates does not match well because of difficulties of precise velocity measurement. More future analysis are still needed for predictions of flow rates.

Chapter 5

Conclusions and future work

5.1 Conclusions

Atriums have been widely used in non-residential buildings for aesthetic requests, social contact, exposure for daylight, and fresh air exchange. The shapes and displacement of atriums are determined by building functions, thermal comfort and ventilation requirements, climates, and daylight performances. Centralized atriums are still the most popular which are basic forms in this study for modeling and simulations. In atrium buildings, natural ventilation could be considered to assist indoor air circulation, maintain suitable thermal environment and avoid or reduce the use of mechanical systems, such as air conditioning. To predict the reduction in energy costs, indoor comfort and possible operations of controlling systems, modeling techniques are needed before the architectural design stage.

Present natural ventilation modeling strategies are classified into four categories: analytical models, full-scale and small-scale experiments, computational fluid dynamics and airflow network models. All methods have advantages and limitations. Analytical models provide rich physical meanings and are easy to be applied, but they are too simple to represent real-world conditions. Full-scale field experiments require much resources which leads to difficulties in collecting sufficient data sets. Small-scale experiments cannot meet the exact match of dimensionless numbers due to the change of geometry. CFD simulations require much computational resources

and cannot show results in long time periods. Moreover, airflow network models are limited by many assumptions including well-mixed temperature conditions in a single zone and negligible momentum of air.

This thesis focuses on study temperature stratification and air circulation inside atrium buildings in purely buoyancy-driven ventilation. Results and conclusions will help designers and engineers predict the indoor comfort and energy savings before design and construction.

Because the investigations on atrium structure features and opening characteristics have been limited up to now. Computational fluid dynamics simulations are used to study the ventilation effects based on comparisons among building models with different heat sources, opening locations, sizes and numbers of layers. The basic building model is a large room with a inlet on the sidewall and the heat source on the ground connected to a centralized atrium with an outlet on the top. In all cases, buoyancy effect drives air to come through the inlet, flow through the connecting opening, float up inside the atrium, and finally flow out from the top outlet. Different heat sources produce similar velocity fields and total flow rates with equivalent heat loads. But the uniformly heated floor shows better mixed temperature distribution than the heater near walls. On the other hand, different locations of the outlets on the top of the atrium show little effects on the temperature and velocity fields. A small window connecting the room and the atrium results in higher velocities and more obvious temperature stratification near the opening than those in models with floor-ceiling openings. Airflow rates are higher while indoor temperatures in both the room and atrium are lower in the building model with a large outlet compared with the case with a small outlet. However, regardless of the outlet sizes and locations, a well-mixed temperature field inside the atrium can be assumed.

Adding the floors of an atrium building enhances natural ventilation. Total airflow rates and temperature increase in the two-layer model are higher than those in the single-layer model. Lower flow rates are observed through the second floor than the first floor with all other parameters are constant, which leads to higher room temperatures. Furthermore, the well-mixed temperature field is still verified in the

lower half of the atrium space while the temperature stratification exists in the upper half. Therefore, the temperature distribution inside the atrium of multi-layer buildings should be carefully considered by accounting for the gradually temperature increase with height.

CoolVent is used as a airflow network tool to compare the results with CFD simulations. Calculations in CoolVent assume uniform air temperatures in every zone and ignore the momentum of air. In comparison with CFD simulations, both temperatures and flow rates match well with discrepancies less than 10%. The well-mixed temperature assumption in the atrium used in the airflow network tool is suitable for single-layer atrium buildings but further calculations should be improved for multi-layer buildings.

A full-scale field experiment is conducted in a five-storey stairwell of MIT Building 35, which could be treated as a simple small atrium. Temperatures of indoor air are measured by thermocouples evenly distributed in the vertical direction while temperatures of inside surfaces are measured by an infrared thermometer. Velocities at the bottom door and top door are measured by hotwire anemometers. Measured flow rates at two doors fluctuate frequently and are not in phase, which may not reflect the real flow rate change during the experiment process. When the opening area are reduced to a half, flow rates decrease less than a half. Solar gains through windows would assist natural ventilation by heating up the walls and stairs. Though the indoor air temperatures on every floor keep stable during the experiment, air temperatures increase with height because the heat transfer with the surfaces when flowing through them. Therefore, the well-mixed temperature assumption over the entire height in many analytical models and airflow network models is not applicable if the cross area of the atrium is small. The temperature stratification should be carefully considered.

More calculations and analysis are provided to predict the flow motions and temperature distributions in buoyancy-driven ventilation in atrium buildings. The considerations of flow resistance, pressure drops, heat transfer coefficients for walls and stairs, and mixed ventilation are discussed in details. When the outside air temperatures and surface temperatures are known, corresponding indoor air temperatures

would be predicted by the heat transfer balance between air and surfaces. Calculated and measured results of temperatures match well. Some errors in the heat transfer coefficient estimation cause the slightly lower temperatures in calculations compared with the actual temperatures in the experiment. In addition, the calculated flow rates are not in phase with measured flow rates through both the bottom door and the top door.

5.2 Future work

There are a few limitations in this research. Additional future work are needed.

The atrium type used in computational fluid dynamics is the centralized atrium connected with rooms. The sizes and locations of openings in the atrium building are chosen to represent the simplest and universal situations. There are more cases where purely buoyancy-driven ventilation is important to meet diverse architectural aesthetics and climates. These cases should be carefully generalized and taken into consideration as well. Based on the comparison between the results of CFD models and CoolVent models, the total air temperature increase and flow rates match well. But the temperature stratification in the room still exists, which requires more analysis to describe besides the simple airflow network model. In multi-layer buildings, temperature field could not be assumed to be well-mixed in the atrium space and disagrees with the CoolVent results. The calculation methods in CoolVent for ventilation in multi-layer atrium buildings should be revised.

The experiment conducted in the stairwell of MIT building 35 provides detailed data sets of actual temperature distributions and air flow rates. However, the measured flow rates at doors are not in phase because of the difficulties in recording velocities fluctuating rapidly and randomly. The Measured outside air temperatures reach an abnormal peak at 10:30 caused by some unknown heat sources. Analysis based on results including these errors is difficult. Additional experiments should be conducted using better automatically recorded anemometers and thermometers.

The calculations in chapter 4 successfully verify the measured results in the ex-

periments and help predict the indoor environment in similar atrium space. But the resistance and pressure drops of the flow process are calculated using empirical values in some handbooks and change in different cases. More future work should be done to determine the resistance coefficients applied in various building structures. Calculated air temperatures keep lower than measured air temperatures during the experiment time period. Some unknown factors in heat transfer coefficient estimation should be investigate carefully. In addition, more full-scale experiments should be conducted in typical atriums besides the experiment in a stairwell in this study.

Bibliography

[1] Hotel hannover-wyndham hotel hannover atrium, 2010-09-30, www.wyndhamhannover.com.

[2] CK Quek. Design of atrium. building in the warm humid tropics. *Unpublished M. Phil. Dissertation. Paris, France: Darwin College Cambridge*, 1989.

[3] Ventilation by atrium http://www.mfe.govt.nz/publications/sus-dev/passive-solar-designguidelines/html/page4.html.

[4] Microdata File. Commercial buildings energy consumption survey (cbecs). 2011.

[5] PF Linden, GF Lane-Serff, and DA Smeed. Emptying filling boxes: the fluid mechanics of natural ventilation. *Journal of Fluid Mechanics*, 212:309–335, 1990.

[6] M Alejandra Menchaca-Brandan, F Alonso Dominguez Espinosa, and Leon R Glicksman. The influence of radiation heat transfer on the prediction of air flows in rooms under natural ventilation. *Energy and Buildings*, 138:530–538, 2017.

[7] IE Idelcik. Handbook of hydraulic resistance. 2003.

[8] J Bednar Michael. The new atrium; 1986.

[9] MR Atif. Atrium buildings: amenities, energy costs and environment. *Construct Canada*, 36:43–47, 1993.

[10] WY Hung and WK Chow. A review on architectural aspects of atrium buildings. *Architectural Science Review*, 44(3):285–295, 2001.

[11] View of central atrium at the domestic terminal of hartsfield-jackson atlanta international airport in atlanta, georgia, usa, 2010-09-30, www.alamy.com/stock-photo-view-of-central-atrium-at-the-domestic-terminal-of-hartsfield-jackson-72593834.html.

[12] Interior of atrium, march 2008, www.commons.wikimedia.org/wiki.html.

[13] Futura atrium european interior landscaping organisation, may 2015, www.eilo.eu/2015/11/futura-atrium.html.

[14] Glass roof panel / laminated / safety sentryglas endesa headquarters atrium du pont safety,www.archiexpo.com/prod/du-pont-safety-glas/product-89604-1510224.html.

[15] Annual Energy Outlook et al. Energy information administration. *Department of Energy*, 92010(9), 2011.

[16] ASHRAE Standard. Standard 55-2010:"thermal environmental conditions for human occupancy"; ashrae. *Atlanta USA*, 2010.

[17] Stephen Douglas Ray. *Modeling buoyancy-driven airflow in ventilation shafts.* PhD thesis, Massachusetts Institute of Technology, 2012.

[18] Shaun D Fitzgerald and Andrew W Woods. The influence of stacks on flow patterns and stratification associated with natural ventilation. *Building and Environment*, 43(10):1719–1733, 2008.

[19] Pei-Chun Liu, Hsien-Te Lin, and Jung-Hua Chou. Evaluation of buoyancy-driven ventilation in atrium buildings using computational fluid dynamics and reduced-scale air model. *Building and Environment*, 44(9):1970–1979, 2009.

[20] Peter V Nielsen. Airflow in a world exposition pavilion studied by scale-model experiments and computational flud dynamics. Technical report, Dept. of Building Technology and Structural Engineering, 1998.

[21] Y Ji, MJ Cook, and V Hanby. Cfd modelling of natural displacement ventilation in an enclosure connected to an atrium. *Building and Environment*, 42(3):1158–1172, 2007.

[22] Yasushi Kondo, Takeshi Ogasawara, and Jun-ichi Fujimura. Interactive simulation of room air temperature and absorption/emission of radiative heat with room moisture. *Air distribution in rooms*, 1:427–432, 2000.

[23] CA Rundle, MF Lightstone, P Oosthuizen, P Karava, and E Mouriki. Validation of computational fluid dynamics simulations for atria geometries. *Building and Environment*, 46(7):1343–1353, 2011.

[24] James Axley. Multizone airflow modeling in buildings: History and theory. *HVAC&R Research*, 13(6):907–928, 2007.

[25] Zhiwen Luo, Jianing Zhao, Jun Gao, and Lixia He. Estimating natural-ventilation potential considering both thermal comfort and iaq issues. *Building and environment*, 42(6):2289–2298, 2007.

[26] PG Rousseau and EH Mathews. A new integrated design tool for naturally ventilated buildings. *Energy and buildings*, 23(3):231–236, 1996.

[27] Maria-Alejandra Menacha-B and Leon Glicksman. Coolvent: A multizone airflow and thermal analysis simulator for natural ventilation in buildings. *IBPSA-USA Journal*, 3(1):132–139, 2008.

[28] PA Favarolo and H Manz. Temperature-driven single-sided ventilation through a large rectangular opening. *Building and Environment*, 40(5):689–699, 2005.

[29] ASHRAE Standard. Ansi/ashrae/iesna standard 90.1-2004. *Energy standard for buildings except low-rise residential buildings*, 2004.

[30] Qingyan Chen. Ventilation performance prediction for buildings: A method overview and recent applications. *Building and environment*, 44(4):848–858, 2009.

[31] Guohui Gan and Saffa B Riffat. Cfd modelling of air flow and thermal performance of an atrium integrated with photovoltaics. *Building and Environment*, 39(7):735–748, 2004.

[32] Cheng Jun. *An Experimental and Computational Study of Natural and Hybrid Ventilation in Buildings*. PhD thesis, Concordia University, 2017.

[33] Stephen D Ray, Nan-Wei Gong, Leon R Glicksman, and Joseph A Paradiso. Experimental characterization of full-scale naturally ventilated atrium and validation of cfd simulations. *Energy and Buildings*, 69:285–291, 2014.

[34] infraredthermometer https://www.ryobitools.com/products/details /infraredthermometer640.

[35] JC Hart, JS Park, and CK Lei. Heat transfer enhancement in channels with turbulence promoters. *Journal of Engineering for Gas Turbines and Power*, 107:628–635, 1985.

[36] Johann Nikuradse. *Laws of flow in rough pipes*. National Advisory Committee for Aeronautics Washington, 1950.

[37] Je-Chin Han, LR Glicksman, and WM Rohsenow. An investigation of heat transfer and friction for rib-roughened surfaces. *International Journal of Heat and Mass Transfer*, 21(8):1143–1156, 1978.

[38] RL Webb, ERG Eckert, and RJf Goldstein. Heat transfer and friction in tubes with repeated-rib roughness. *International Journal of Heat and Mass Transfer*, 14(4):601–617, 1971.

[39] SW Churchill and R Usagi. A general expression for the correlation of rates of transfer and other phenomena. *AIChE Journal*, 18(6):1121–1128, 1972.

[40] Stuart W Churchill and Humbert HS Chu. Correlating equations for laminar and turbulent free convection from a vertical plate. *International journal of heat and mass transfer*, 18(11):1323–1329, 1975.

[41] SW Churchill. Combined free and forced convection around immersed bodies, heat exchanger design handbook. 2002.